GEOLOGICA CARPATHICA, 2025, 76, 6, 417–444 https://doi.org/10.31577/GeolCarp.2025.24

The tectonic evolution of the Transdanubian Range: Insights from Strázsa Hill (Zsámbék town), a key outcrop in the central Pannonian Basin

GÁBOR HÉJA[1,✉], ZSOLT KERCSMÁR[1], TAMÁS BUDAI[2], MÁRTON PALOTAI[1], PÉTER KÓNYA[1], ZOLTÁN LANTOS[1], SZILVIA KÖVÉR[3,4], BARBARA BEKE[4] and LÁSZLÓ FODOR[3,4]

[1]Supervisory Authority for Regulatory Affairs, Geological Survey, 1123 Budapest, Alkotás utca 50, Hungary
[2]University of Pécs, Department of Geology and Meteorology, 7624 Pécs, Ifjúság útja 6, Hungary
[3]HUN-REN Institute of Earth Physics and Space Sciences, 9400 Sopron, Csatkai E. u. 6–8, Hungary
[4]Eötvös University, Institute of Geography and Earth Sciences, Department of Geology, 1117 Budapest, Pázmány Péter sétány 1/C, Hungary

(Manuscript received August 26, 2025; accepted in revised form December 4, 2025; Associate Editor: Rastislav Vojtko)

Abstract: The Strázsa Hill quarry is an exceptional outcrop in the central part of the Pannonian Basin. It exposes one of the major structures of the Transdanubian Range, the Vértessomló thrust. In this study, we investigated Strázsa Hill from a structural point of view, documenting its complex structural evolution through interpreted outcrop photographs and fault slip analysis. Our findings show that the exposed part of the Vértessomló thrust comprises an imbricate system of south-vergent thrust sheets composed of Middle and Upper Triassic rocks. Major thrusting occurred before the Middle Eocene, most probably during the mid-Cretaceous. Sedimentological and structural evidence at Strázsa Hill indicates that the thrusts underwent dextral-reverse reactivation during the Oligocene, resulting in the formation of a growth syncline in the footwall. The Vértessomló thrust and associated E–W striking structures were later overprinted by several NW–SE to N–S striking normal faults during the Middle to Late Miocene. Some of these faults were reactivated during neotectonic strike-slip faulting. Our observations provide an important basis for understanding the tectonic evolution of the northern part of the Transdanubian Range.

Keywords: Eoalpine thrust, Hungarian Paleogene basin system, oblique reactivation, Miocene extension

Introduction

Remarkable outcrops hold significant value in geosciences. They represent an essential part of our geoheritage, attract geotourists (e.g, Mahboubi & Naimi 2024; Sotiriou & Nunes 2024), and may host exceptionally well-preserved fossils (Főzy & Janssen 2009; Erdei et al. 2022), stunning minerals, or rock successions that preserve crucial geohistorical information (Keller et al. 1995). From a tectonic perspective, key outcrops are particularly valuable, as they can provide insights into the age and kinematics of deformation (Palotai et al. 2017; Granado et al. 2018). Well-exposed outcrops are especially important in regions with generally poor exposure conditions, such as flat-lying sedimentary basins.

In this study, we present the complex and well-preserved structural assemblage of Strázsa Hill, located in the central part of the Pannonian Basin (Fig. 1A). This area has been extensively investigated by numerous boreholes drilled for coal and bauxite exploration (Véghné Neubrandt et al. 1978; Héja et al. 2022). However, the study of surface outcrops is challenging due to the widespread Quaternary cover deposits and the generally poor exposure of pre-Quaternary formations. Strázsa Hill stands out as a key locality in the central Pannonian Basin, where various Triassic rocks are exposed together with thin remnants of Oligocene and Miocene successions. Previous studies have mainly focused on the stratigraphy, sedimentology, and paleontology of this outcrop (Budai 2004; Farics 2018; Dunkl et al. 2019; Kercsmár et al. 2020; Erdei et al. 2022), whereas its Eoalpine structure was discussed in a broader regional context by Budai et al. (2015).

Our study presents a detailed structural analysis of Strázsa Hill, including tectonic interpretation of outcrop photographs and fault-slip analysis. Based on these datasets, we reconstructed the structural evolution of the study area from the Triassic Neotethyan rifting, through Cretaceous Eoalpine shortening, Paleogene strike-slip faulting, and Miocene extension, to neotectonic inversion. Several identified structures refine previous interpretations of the structural geometry, fault kinematics, and timing of deformation. Our observations also provide a basis for the structural interpretation of the dense network of well data of the surrounding area (Héja et al. 2022).

Geology of the study area

The Mesozoic succession of Strázsa Hill forms part of the Transdanubian Range (TR), which represents the uppermost thick-skinned nappe of the Austroalpine nappe pile (Figs. 1A,

✉ corresponding author: Gábor Héja
gabor.heja@sztfh.hu

2A) (Tari 1994; Schmid et al. 2008; Fodor et al. 2017). The TR was located along the passive margin of the Neotethys Ocean following its Anisian break-up (Haas et al. 1995). The Middle to Upper Triassic passive-margin succession of the TR is dominated by shallow-marine dolostones that include deep-marine intercalations (Budai et al. 2015) (Fig. 1D). The oldest exposed rock at Strázsa Hill is the late Anisian–Ladinian Budaörs Formation, consisting of thick-bedded shallow-marine dolostones containing a Diplopora annulata green algae assemblage (Haas et al. 1981; Budai 2004; Budai et al. 2015). A partly heterotopic deep-marine succession of cherty limestones and volcanoclastic sediments ("Buchenstein Group") was intersected by several boreholes (Mány M-191, M-245, M-246, Figs. 1D, 2B) north of the quarry (Budai 2004). Coarse-grained volcanoclastic rocks and altered tuffs of the Inota Formation are exposed at Strázsa Hill, representing the younger part of the "Buchenstein Group" (Budai et al. 2015). Zircon U–Pb geochronological data indicate an Early Carnian age (232 Ma) for these volcano-sedimentary rocks (Dunkl et al. 2019) (Fig. 1D).

The "Buchenstein Group" is overlain by the progradational tongue of the shallow-marine Gémhegy Dolomite (Fig. 1D), which, in turn, is overlain by Carnian deep-marine cherty limestones and dolostones of the Csákberény Formation (Budai et al. 2005). These formations are not exposed at Strázsa Hill but are known from boreholes north of the studied outcrop (e.g., Zsámbék Zs-14, Fig. 2B) (Haas et al. 1981). The intertidal dolostones of the Fődolomit Formation (equivalent to the Hauptdolomit or Dolomia Principale in the Alps) were deposited from the Late Carnian to the Late Norian (Haas et al. 1995). The Fődolomit is overlain by the shallow-marine uppermost Norian to Rhaetian Dachstein Limestone (Fig. 1D). The Fődolomit is exposed at Strázsa Hill (Budai et al. 2015), whereas the transitional beds between the Fődolomit and Dachstein Limestone have been intersected by several boreholes in the surrounding area (Héja et al. 2022).

The upper part of the Mesozoic succession is absent in the Strázsa Hill area due to subaerial erosion associated with Cretaceous folding, thrusting, and subsequent uplift (Tari 1994; Kaiser 1997; Fodor et al. 2018). The Triassic succession of the study area was imbricated by south-vergent thrusts (Héja et al. 2022), a deformation phase linked to the Cretaceous Eo-Alpine orogeny that developed between the Alpine Tethys and the Neotethys Oceans. One of the most significant related structures is the Vértessomló "line" (Balla & Dudko 1989) (Fig. 2B), which has been previously interpreted as a south-vergent Cretaceous thrust in its western segment (Császár et al. 1978; Császár 1995; Fodor & Bíró 2004) or as a Cenozoic strike-slip fault (Balla & Dudko 1989). The Vértessomló "line" crosses Strázsa Hill with an approximately E–W strike (Budai et al. 2015; Héja et al. 2022).

The tilted Triassic beds are unconformably overlain by the deposits of the Hungarian Paleogene Basin (Fig. 1D), which is interpreted as a retroarc foreland basin developed in the hinterland of Carpathian orogenic wedge (Báldi-Beke & Báldi 1985; Tari et al. 1993) (Fig. 1B). Although the older, Eocene part of this succession is absent in the Strázsa Hill area, late Middle Eocene deposits are widespread north of the E–W-striking Paleogene Környe–Zsámbék fault, located a few hundred metres north of the quarry (Fig. 2B) (Véghné Neubrandt et al. 1978; Balla & Dudko 1989; Fodor 2008; Héja et al. 2022). This fault delineates the southern margin of the Eocene deposits (Figs. 1B, 2B). Strázsa Hill is situated on the southern side of the northward-stepping Környe–Zsámbék fault, where the Triassic formations are directly covered by Oligocene and Miocene beds (Kercsmár et al. 2020; Erdei et al. 2022) (Fig. 2B). Following Early Oligocene uplift and weathering (Kelemen et al. 2023), terrestrial to marginal marine sedimentation of the North-western Transdanubian Paleogene Basin extended southward over the study area during Early to Late Oligocene (Fig. 1D). The Oligocene succession begins with red terrestrial clay and bauxite of approximately 31 Ma (Óbarok Fm.) (Kelemen et al. 2023), overlain by the Csatka Fm. and the Mány Mb. of the Törökbálint Fm. The Csatka Fm. consists of clay with thin coal seams and coarse-grained pebbly sandstones, deposited in alluvial, paludal, and lacustrine environments. The Mány Mb. comprises various siliciclastic sediments (clay, siltstone, sandstone, and conglomerate) that were deposited in the transition zone between deltaic and shallow-marine environments (Báldi 1986) (Fig. 1D). Erdei et al. (2022) described several plant fossils from the Oligocene succession exposed in the quarry. The study area experienced uplift and subaerial exposure during the Early Miocene (Fig. 1D).

The Miocene sedimentation was controlled by syn-sedimentary grabens and half-grabens associated with the opening of the Pannonian back-arc basin (Fig. 1C). The continental siliciclastic succession of the early Middle Miocene Perbál Fm. is overlain by Middle Miocene marine clays and marls (Baden and Kozárd fms.) (Fig. 1D). At the same time, the late Middle Miocene shallow-water Tinnye Limestone was deposited on the elevated areas and prograded over basinal formations (Cornée et al. 2009; Palotás 2014). The clays and silts of the Csákvár Mb. of the Endrőd Marl Fm. were deposited during the Late Miocene in swamp environments (Csillag et al. 2008; Sztanó et al. 2024). Strázsa Hill is located at the footwall edge of a map-scale, N–S-striking Miocene normal fault (Héja et al. 2022) (Fig. 2B), which is expressed in the morphology of the hill as a topographic step. Consistent with this structural position, the Middle Miocene succession at Strázsa Hill is represented by a 10–12 m thick, condensed sequence of shallow-marine and lagoonal deposits. This succession is characterised by the predominance of fine-grained siliciclastic sediments with limestone intercalations (Kercsmár et al. 2020), in contrast to the area immediately north of the quarry, where the Middle Miocene is represented by more than 50 m of oolitic limestone of the Tinnye Fm. The Middle Miocene succession at Strázsa Hill is unconformably overlain by a one-meter-thick freshwater limestone bed (referred to herein as the Upper Miocene basal bed), which is considered the basal bed of the Csákvár Mb. (Kercsmár et al. 2020) (Fig. 1D).

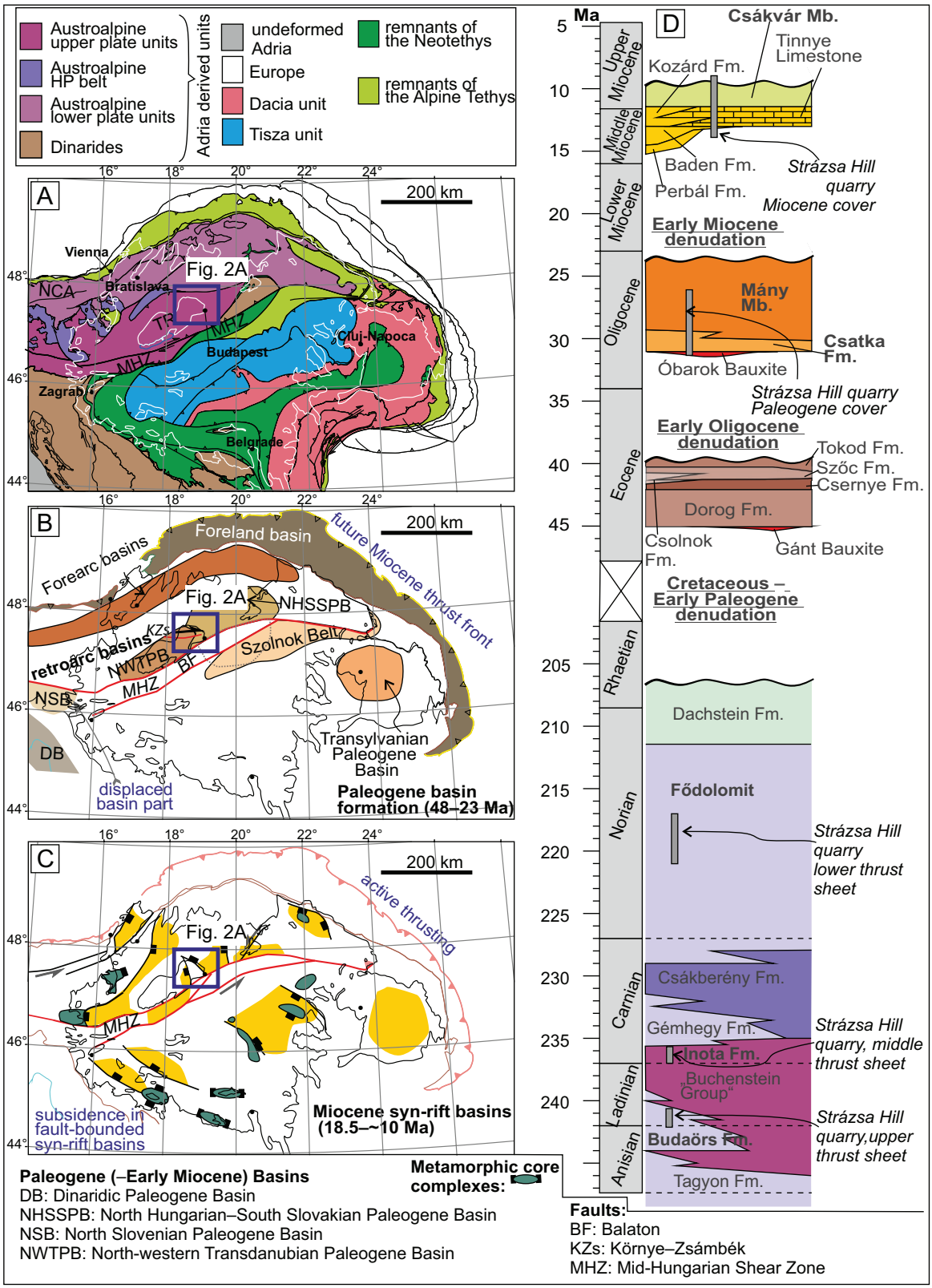

Fig. 1. Location of the study area in the Alpine–Carpathian–Pannonian–Dinaridic system during different stages of structural evolution. **A** — Main tectonic units of the basement of the Pannonian Basin after Schmid et al. (2008). NCA: Northern Calcareous Alps; MHZ: Mid-Hungarian Zone; TR: Transdanubian Range. **B** — Simplified map of Paleogene basins. Note the Early Miocene separation of the Hungarian and Slovenian Paleogene basin parts. **C** — Position of the Zsámbék Basin in the Miocene Pannonian back-arc basin. B–C is after Fodor et al. (2013) modified, using the data of Tari et al. (1993), Kázmér et al. (2003), and Csontos et al. (2025). **D** — Stratigraphic column of the Zsámbék and Mány Basins highlighting the units exposed in the Strázsa Hill (after Héja et al. 2022, modified).

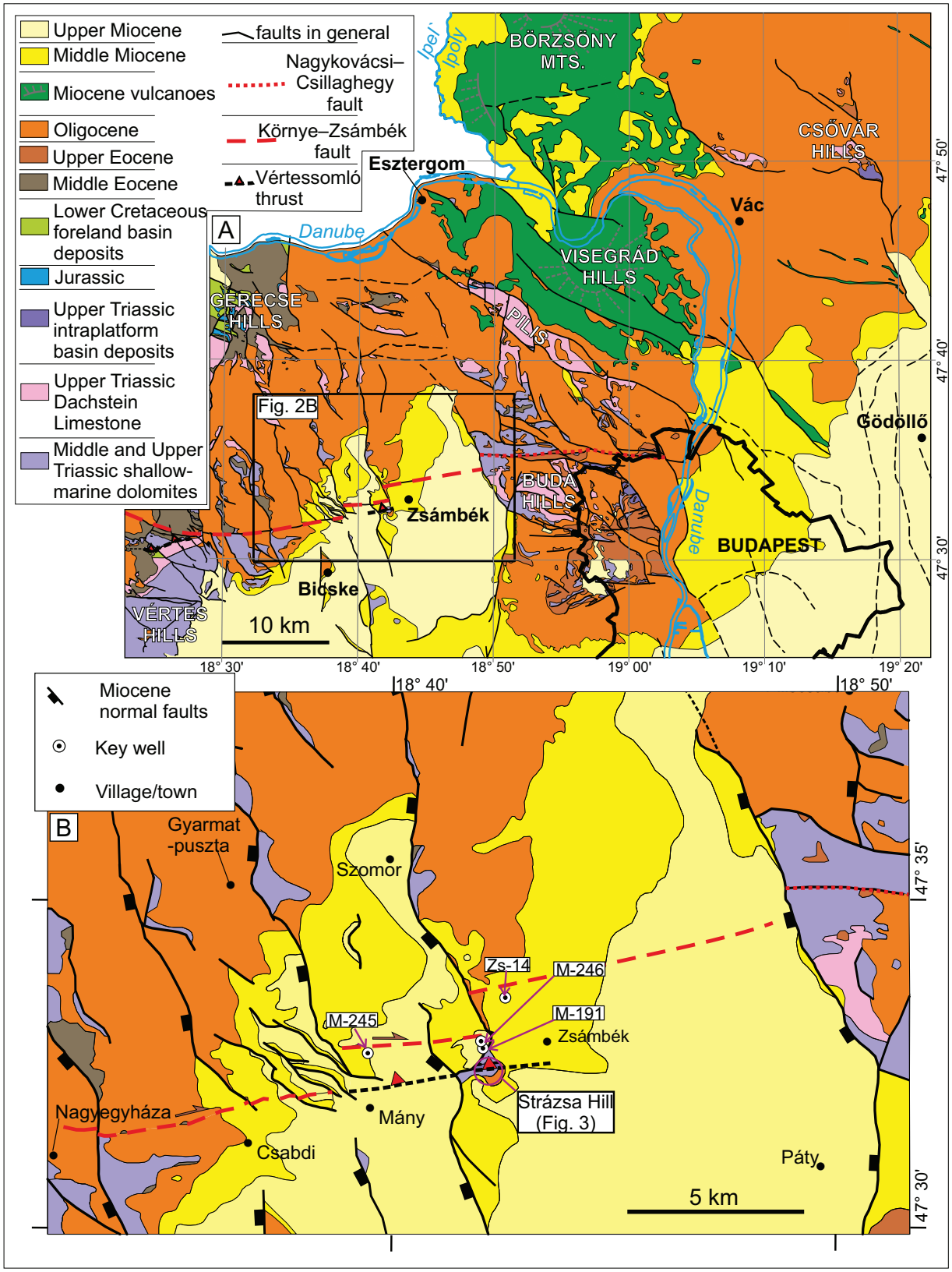

Fig. 2. A — The position of the Zsámbék and Mány Basins on the pre-Quaternary geological map of the northeastern TR. The map is based on the works of Wein (1977), Balla & Dudko (1989), Fodor et al. (1994), Prakfalvi et al. (2000), Scharek et al. (2000), Karátson & Németh (2001), Budai & Síkhegyi (2004), Császár et al. (2004), Fodor et al. (2018), Budai et al. (2018), and Héja et al. (2022). For the location of the map, see Fig. 1A–C. **B** — Location of Strázsa Hill and the relevant surrounding wells on the Pre-Quaternary geological map of Zsámbék and Mány Basins, based on Héja et al. (2022), modified. For the location of the map, see Fig. 2A.

During the Pliocene and Quaternary, the TR was uplifted and subaerially exposed. Various continental sediments were deposited during this time, including proluvial, alluvial, fluvial, and aeolian deposits.

Methods and data

Detailed geological and structural mapping was carried out at Strázsa Hill (Fig. 3A). Outcrop photographs and UAV-based imagery were used for photogrammetry and structural interpretation. The 3D model of the most significant parts of the quarry was constructed using Agisoft Metashape software.

Several types of structural data were measured at Strázsa Hill, including bedding dips, faults with and without striae, and sedimentary dykes (Fig. 3B). These data were analysed using the software package of Angelier (1990). Structural data were plotted on stereonets using a lower-hemisphere equal-area (Lambert) projection. For faults lacking slickenlines, the principal stress axes were estimated "manually", following Anderson's theory of conjugate fault sets (Anderson 1951). Fault-slip inversion and automatic separation based on fault-slip data were performed using the method of Angelier & Manoussis (1980).

Several types of cross-cutting relationships were considered when determining the relative sequence of deformation phases. Tilt tests were performed on tilted conjugate fault pairs (Angelier 1990). During these tests, the structural elements were back-tilted to restore the bedding to its original horizontal position. If the symmetry plane of a conjugate fracture set appeared vertical or horizontal on the back-tilted stereonet, the fault set was assumed to have formed before the tilting of the beds. Oblique striae were interpreted as pre-tilt structures if the lineation displayed pure dip-slip or strike-slip kinematics after the tilt test. In cases where the tilt test results were inconclusive, oblique striae were considered as second-phase reactivation of an older fault that originally showed pure dip-slip or strike-slip motion.

Structural description of Strázsa Hill

Eastern wall, northern part

The Vértessomló thrust (also referred to as Vértessomló–Nagykovácsi line; Balla & Dudko 1989) is one of the major Cretaceous thrusts of the TR. It is exposed on the eastern wall of the quarry (Figs. 3A, 4B,G). In this section, the older Carnian Inota Fm. is thrust over the latest Carnian–Norian Fődolomit Fm. The thrust dips steeply (~60°) to the north, whereas the footwall is composed of gently (~20–30°) north-dipping beds of the Fődolomit Fm. (Fig. 4B,G). The cut-off angle of the thrust and the footwall bedding is approximately 30° (Fig. 4G). The beds of the Inota Fm. are parallel to the thrust surface in the middle part of the eastern wall, dipping steeply (~50–60°) toward the north (Fig. 4B). Although the original geometry represents an old-on-younger thrust contact, oblique dextral-normal slickenside lineations were observed on the Vértessomló thrust surface, suggesting post-thrust reactivation under a transtensional tectonic regime (Fig. 4D).

An approximately 10 m thick, north-dipping dolostone body occurs within the Inota Fm. This body is interpreted as a progradation tongue of a coeval carbonate platform (Fig. 4B). The dolostone unit is dissected by faults F1 and F2 (Fig. 4B). The southern boundary of the dolostone body is defined by a WNW–ESE-striking, subvertical fault plane with dextral striae (F2; Fig. 4E). This fault cuts the north-dipping Triassic beds and appears to have formed after their tilting.

The footwall of the NE-dipping F1 fault (Fig. 4J) consists of dolostone, whereas the hanging wall is composed of thick green tuffitic clay with coarse-grained volcanoclastic intercalations; the lithologies that are absent in the footwall (Fig. 4H,I). The gently north-dipping beds of the dolostone body are overlain by a subhorizontal thin clay layer, indicating a slight angular unconformity. This clay layer is, in turn, overlain by a dolostone bed that seals both the footwall and the hanging wall of the F1 fault (Fig. 4I). The sealing dolostone bed is dissected by several slide planes, resulting in minor layer rotation (Fig. 4I).

North of the outcrops around the F1 and F2 faults, south-dipping sub-vertical dolostones are exposed, interbedded with green tuffs and brown claystones (Fig. 4B). This succession is interpreted as the uppermost part of the Budaörs Dolomite Fm. We propose that the Budaörs Dolomite was thrust over the Inota Fm. along the northern splay of the Vértessomló thrust (Fig. 4B). However, this inferred tectonic contact is obscured by quarry debris and cannot be directly observed.

Steep to moderately dipping Triassic beds of the Inota Fm. are unconformably covered by the Oligocene red clay along the northern part of the eastern quarry wall, within the hanging wall of the Vértessomló thrust (Fig. 4B). In this area, NNE- and NW-plunging reverse slickenlines were observed on a redeposited dolostone block, approximately 1 m in diameter, enclosed within the red clay (F3 and F4 on Fig. 4B, E). These kinematic indicators were included in fault-slip analysis; however, it remains uncertain whether the related slickenlines were formed before or after the redeposition of the dolostone block.

Eastern wall, southern part

In the footwall of the Vértessomló thrust, along the southern part of the eastern wall, the Fődolomit Fm. is directly overlain by the Csatka Fm. across an angular unconformity (Figs. 4B,G, 5). In this part of the quarry, the Csatka Fm. begins with a thin layer of dolostone breccia (L1) that rests on the erosional surface of the Triassic basement. The dolostone breccia is overlain by a 2–4 m thick, variegated succession of siltstone and clay containing local coal and gypsum intercalations (L2 on Fig. 5).

Above this, a 1–1.5 m thick, cross-bedded layer (L3) consists of purple, coarse-grained sandstone and conglomerate

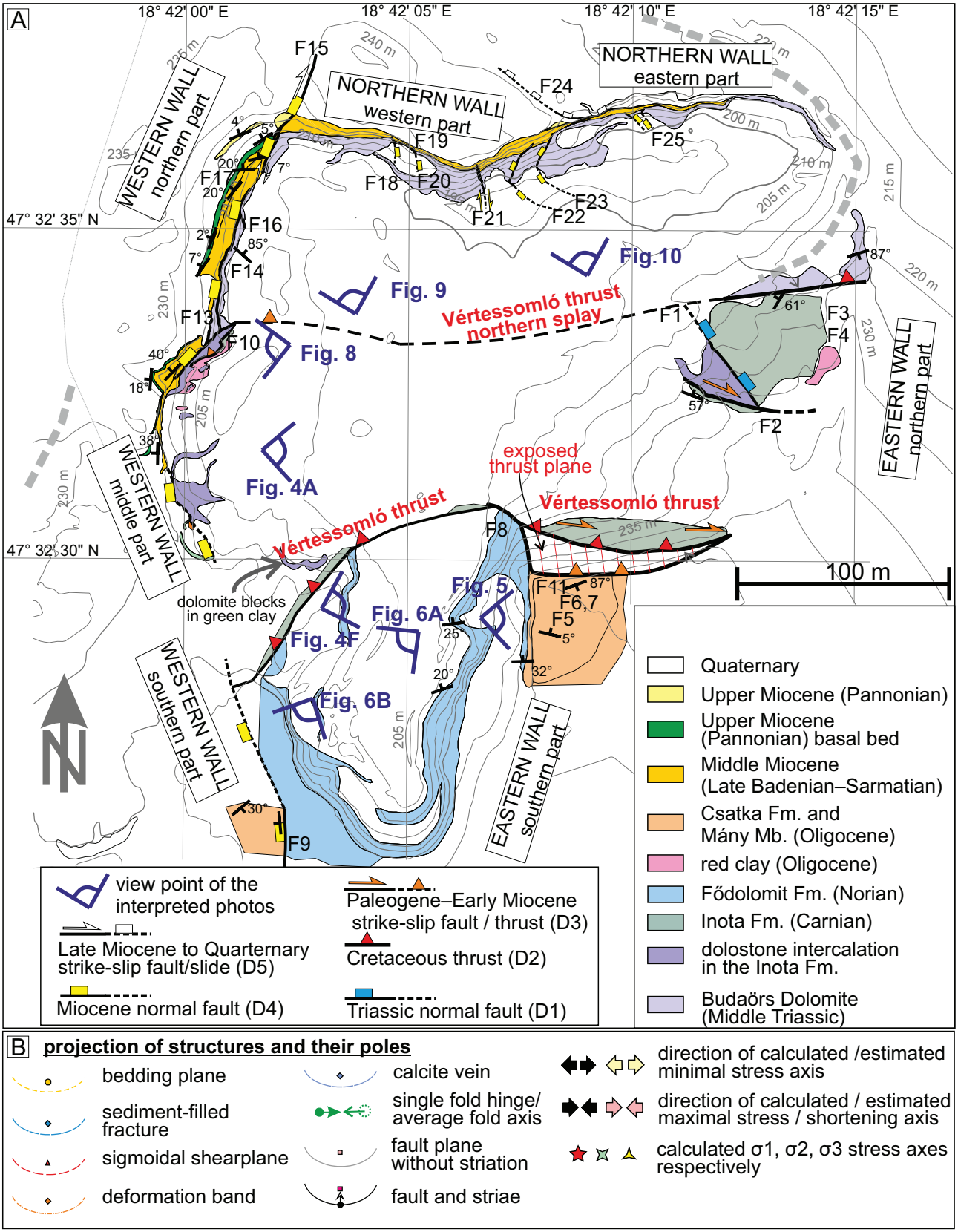

Fig. 3. A — Geological map of Strázsa Hill. For the location of the quarry, see Fig. 2B. F1–25: studied faults. **B** — Legend of the stereoplots in Figs. 4–6 and in Figs. 8–11.

with red clay matrix (Fig. 5). The clasts are derived from the local Triassic dolostones, whereas the matrix is composed of reworked Oligocene red clay. The base of this coarse-grained layer is characterised by bulge and lobe structures, forming simple load casts produced by rapid accumulation of coarse-grained sediment (Fig. 5E). Water-escape structures are also present within the coarse-grained deposits (Fig. 5E).

These coarse-grained sediments are covered by grey, clayey silt (L4) containing plant fossils (Erdei et al. 2022). The overlying marine succession of the Mány Mb. begins with red, coarse-grained sand (L5) followed by fine-grained sand and silt (L6–8 on Fig. 5). Abundant Ophiomorpha trace fossils (3–5 cm in diameter) occur near the facies boundary and form a distinct horizon within the coarse-grained sand layer. A 5 m thick and 20 m wide channel cuts into this succession along an erosional unconformity (Fig. 5A, B). The channel, striking approximately E–W and parallel to the Vértessomló thrust, is filled with cross-bedded sand in a red clay matrix (Fig. 5A, B). Additional thin intercalations of red sandstones occur near the top of the Oligocene succession.

Beds of the Csatka Fm. and the Mány Mb. dip gently toward the ESE in the southern part of the eastern quarry wall. Approaching the Vértessomló thrust, these beds progressively steepen, becoming subvertical and locally overturned (Fig. 5A, B, F, J). The geometry of the Oligocene beds thus defines an asymmetric footwall syncline in the front of the Vértessomló thrust (Fig. 5A, B, F). The tectonic contact between the Triassic Inota Fm. and the Oligocene succession is represented by a poorly exposed, chaotic zone that formed due to deformational mixing of the two clay-rich lithologies (Fig. 5F). Near this contact, the variegated clay at the base of the Oligocene succession (L2) is overturned and steeply dips northward (Fig. 5B, F). Above it, the coarse-grained sand and gravel beds (L3) dip steeply southward, onlapping the overturned clay layer (Fig. 5F). The coarse-grained sand and conglomerate beds are covered by moderately south-dipping clay and siltstone beds, which thicken toward the core of the footwall syncline (L4 on Fig. 5A, B, F).

Above these, the red coarse-grained sand beds are vertically dragged along the Vértessomló thrust (Fig. 5A). The steeply south-dipping Oligocene beds are dissected by the F6 fault pair (Fig. 5C). The tilt-test results indicate that the F6 faults represent a set of conjugate thrusts that developed before the folding of the Oligocene beds (Fig. 5G, H). In addition, several NW–SE-striking dextral faults and steeply NE-dipping dextral-reverse faults with oblique slickenside lineations (F11 fault set on Fig. 5I) cut the steeply dipping to overturned limb of the footwall syncline (Fig. 5F). A gently north-dipping F7 thrust with only a few centimetres of displacement dissects the moderately south-dipping beds of the Mány Mb. (Fig. 5D). South of the main thrust, dextral-reverse slickenlines were measured on a north-dipping fault (F5 on Fig. 4B, E) that dissects the subhorizontal beds of the Mány Mb. Two N–S-striking sinistral faults were also identified in the Fődolomit Fm. in the lower part of the eastern quarry wall (F8 on Fig. 4B, E).

Western wall, southern part

The southern pit of the quarry consists of gently north-dipping (20–30°) beds of the Fődolomit Fm. (Fig. 3A). On the southern part of the western wall, the Oligocene Mány Mb. is downthrown along the steeply WSW-dipping F9 fault (Fig. 6A, B). In the hanging wall of the F9 fault, the Mány Mb. consists of an approximately 6 m thick succession of thick-bedded brown clayey sandstone, conformably covered by a one-meter-thick red clay layer and a one-meter-thick green clay bed (Fig. 6B). This succession is overlain, with an angular unconformity, by an approximately 2-meter-thick clast-supported breccia body composed of redeposited dolostone clasts (Fig. 6B). Based on our interpretation, the red and green clay layers belong to the Oligocene succession, whereas the overlying breccia either represents the basal breccia of the Miocene succession or is of Quaternary age.

The beds of the Mány Mb. dip towards the southeast in the hanging wall of the F9 fault; however, in the vicinity of the fault, the Oligocene beds dip westward or southwestward due to normal drag along the fault plane (Fig. 6B, F). The red clay layer pinches out towards the F9 fault, and both the clayey sand and green clay are steeply smeared along the fault surface (Fig. 6A, B). In several places, the green clay is injected into the overlying breccia body along ~0,5 m wide, upward-thinning diapir-like structures (Fig. 6B). The core of the F9 fault is represented by a 20–30 cm wide zone where angular, oriented brown clayey sand clasts of the Mány Mb. occur within a powdered dolostone matrix (Fig. 6B, C). Within the contact zone, some faults are verticalized and display oblique striae. Based on their tilt-test results, these striae are interpreted as pre-tilt dip-slip structures (Fig. 6G, H).

North of the F9 fault, the Fődolomit Fm is bounded by a moderately NNW-dipping tectonic contact (Fig. 6A), along which brownish-green clay is smeared (Fig. 6D). The structure can be traced along the quarry floor, where it connects with the Vértessomló thrust exposed on the eastern wall. The clay is overlain by strongly fractured, powdered dolomite (Fig. 6A) and grain-supported breccia composed of up to meter-sized dolostone blocks set within a green clay matrix. We interpret this succession as belonging to the Inota Fm., which contains dolostone intercalations. This relationship indicates that the NNW-dipping contact between the Fődolomit Fm. and the Inota Fm. represents the western continuation of the Vértessomló thrust (Fig. 3). Notably, the thrust exhibits a moderately different strike here – WSW–ENE (Fig. 6I) – compared to the eastern wall, where it strikes E–W (Fig. 4D). The lower contact of the Vértessomló thrust, between the clay and the Fődolomit Fm., is a sharp surface, whereas the upper contact is irregular and appears to be dissected by steeply to moderately NE-dipping faults (F26 and F27) with unknown kinematics (Fig. 6D, I). These faults (F26, F27) detach on the Vértessomló thrust (Fig. 6D).

NW–SE striking individual deformation bands were observed in the sandstone units of the Mány Mb. within the hanging wall of the F9 fault (Fig. 6B). The two samples show

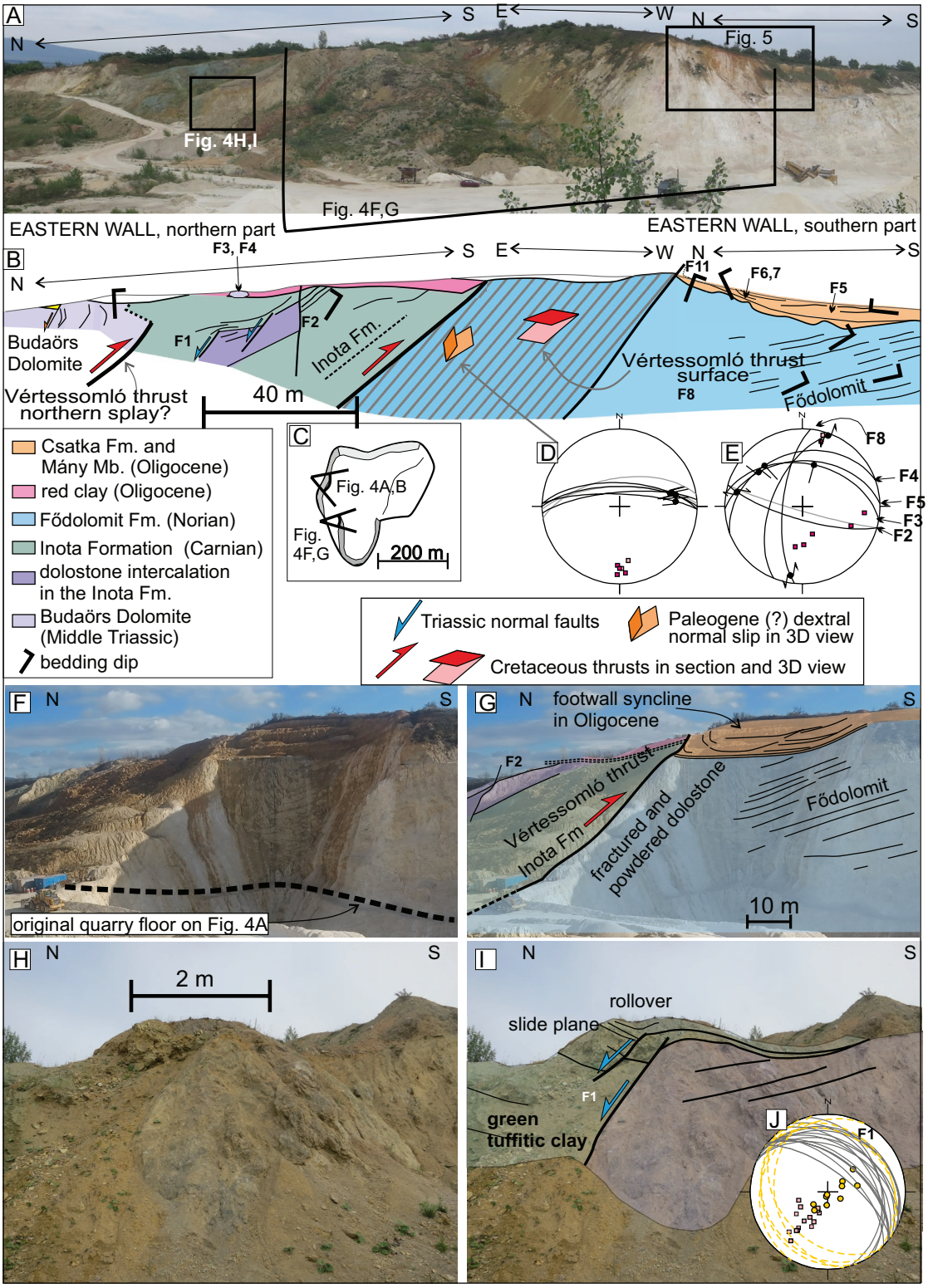

Fig. 4. Structures of the eastern quarry wall of Strázsa Hill: **A** — uninterpreted and **B** — interpreted photos of the eastern wall (for location of the viewpoint see Fig. 3A and Fig. 4C); **C** —point of view of Fig. 4A, B, F and G on the simplified map of the quarry; **D** — oblique dextral-normal slickenlines on the Vértessomló thrust and their stereographic projections; **E** — fault-slip data of the eastern wall (for location of the measurements see Fig.3A and Fig. 4B); **F** — uninterpreted and **G** — interpreted photos of the Vértessomló thrust on the eastern wall (for location of the photo see Fig. 4A, C). Note that Figs. 4A and F were taken at different stages of exploitation. The quarry floor is deeper in Fig. 4F, while the level of the original quarry floor shown in Fig. 4A is indicated on Fig. 4F by a dashed line. **H** — Uninterpreted and **I** — interpreted photos of the F1 Triassic syn-sedimentary normal fault (for location of the photos see Fig. 4A); **J** — stereoplot of F1 fault set (for legend of the stereoplots see Fig. 3B).

slightly different characteristics in terms of kinematics and deformation mechanism. The host rock of sample Zsam20-14a is a quartz-rich sandstone, cemented by calcite (Fig. 7A, B), whereas in sample Zsam20-14b the pores of the quartz-rich sandstone are filled by kaolinite, subordinately silica (chalcedony?), and ferrigenous minerals (Fig. 7C–E). In thin section, deformation band Zsam20-14a shows oversized pores with fine-grained calcite cement infilling between detrital grains, indicating penecontemporaneous dilation and cementation (Fig. 7A, B). Such microstructures are characteristic of dilation bands (Du Bernard et al. 2002). In contrast, band Zsam20-14b exhibits shear-induced grain reorganization, grain rotation, and particulate flow associated with reduced porosity. This band is therefore classified as a compactional shear band. The pores are filled with kaolinite, which may be partly detrital in origin, as kaoline is a typical detrital mineral of the base of the Oligocene sequence (Fig. 7C–E).

Western wall, middle part

Further north, in the central part of the western quarry wall, poorly preserved, powdered dolostone crops out and is surrounded by debris (Fig. 3A, left side of Fig. 8A, B). The age of this block is uncertain; however, based on its structural position – between the two splays of the Vértessomló thrust – it is interpreted as an intercalated dolostone unit belonging to the Inota Fm. Red clay occurring north of the powdered dolostone block was analysed by Gerinczy (2009) using X-Ray diffractometry. According to that study, kaolinite is the only clay mineral present, and the red clay represents the basal formation of the Oligocene succession. The contact of the red clay and the dolostone block is not exposed. Several redeposited dolostone blocks, up to 2 m in size, also occur within the red clay (Fig. 8B). A few decimetre-wide, NW-dipping thrusts with well-developed slickenlines are observed in the surrounding red clay (F10 on Fig. 8B, D). The northern boundary of the red clay is defined by a moderately NNW-dipping fault zone, along which the red clay is juxtaposed against greenish-brown clay containing dolostone intercalations and Budaörs Dolomite Fm. The mineral composition of the green clay (Gerinczy 2009), closely resembles that of the Inota Fm. Therefore, we correlate this fault zone with the northern splay of the Vértessomló thrust (Figs. 3A, 8B), along which the Inota Fm. is smeared between the Oligocene red clay and the Budaörs Dolomite Fm. (Fig. 8B). Bedding of the Budaörs Dolomite Fm. is poorly visible, but locally it is subvertical (040°/85°), similar to observations from the northern part of the eastern wall (Fig. 4B).

A 20–50 cm wide band of brownish-green clay is sheared between two dolostone blocks along the northernmost segment of the northern splay of the Vértessomló thrust (Fig. 8C). Within this NW-dipping sheared clay zone, moderately ENE-dipping sigmoidal shear fractures indicate normal-sense displacement along the fault (Fig. 8D). Further north, the contact between the Triassic and Miocene deposits appears as a wavy, subhorizontal line, representing the intersection of the western quarry wall with the plane of the F13 and F14 faults, which strike subparallel to the wall (Figs. 3A, 8B, E). Locally, the west-dipping, polished fault core of the F14 fault is exposed (banded white planes on Fig. 8B). Dip-slip slickenlines occur on this fault surface near the top of the wall, and their orientations are shown in Fig. 8E. The southern segment of the F13 fault is hosted within the Budaörs Dolomite Fm. (Fig. 8B). Both the F13 and the F14 faults terminate against the surface of the NW-dipping northern splay of the Vértessomló thrust (Fig. 8B). Based on this geometry, the northern segment of the Vértessomló thrust is interpreted as a connecting splay between the two N–S trending normal faults, suggesting its extensional reactivation (Fig. 3A). South of their intersection, the unified normal fault continues and causes the moderate westward tilt of the Miocene layers in the hanging wall (Fig. 3A).

Western wall, northern part

The F15 fault cuts through the entire Miocene succession in the northwestern corner of the quarry (Figs. 3A, 9B). Similar to the F13 and F14 faults, the west-dipping F15 fault strikes subparallel to the western wall (Fig. 3A). The Miocene succession in the hanging wall of the F15 fault was described by Kercsmár et al. (2020). According to their study, the sequence is dominated by Middle Miocene (late Badenian) beds, overlain by a thin layer of late Middle Miocene (Sarmatian) and the Upper Miocene basal bed. A 3-meter-thick succession of sandy silt with redeposited dolostone debris, overlying the Upper Miocene basal bed (Fig. 9E), was interpreted by Kercsmár et al. (2020) as Quaternary in age; however, an older, Late Miocene age cannot be excluded. The Middle Miocene beds and the Upper Miocene basal bed dip gently northward in the hanging wall of the F15 normal fault but are dragged into moderately west-dipping orientation near the F15–F14 fault zone (Fig. 9B, D). Within the overlying unit of uncertain Late Miocene or Quaternary age, the uppermost strata are subhorizontal and onlap the underlying, gently north-dipping beds (Fig. 9E).

The position and drag of the downthrown Miocene strata suggest normal slip along the F15 fault (Fig. 9B, D), which is also supported by several striated fault planes (Fig. 9G). A close-up view of the F15 fault zone (Fig. 9D) shows that fault segments bound a lens composed of dark grey, clayey fine-grained sand. According to Kercsmár et al. (2020), poorly preserved Middle Miocene (Badenian and Sarmatian) microfossils are present within the fault-lens material, interpreted as redeposited bioclasts.

Numerous brittle structures were measured on the limestone intercalations of the Middle Miocene succession and on the overlying Upper Miocene basal bed (F17 fault set on Fig. 9B, F). These subvertical faults strike N–S and NE–SW and exhibit subhorizontal striae. Based on kinematic indicators, fault striations, and en echelon calcite veins, they are interpreted as conjugate dextral and sinistral strike-slip faults formed during NNE–SSW contraction accompanied by perpendicular

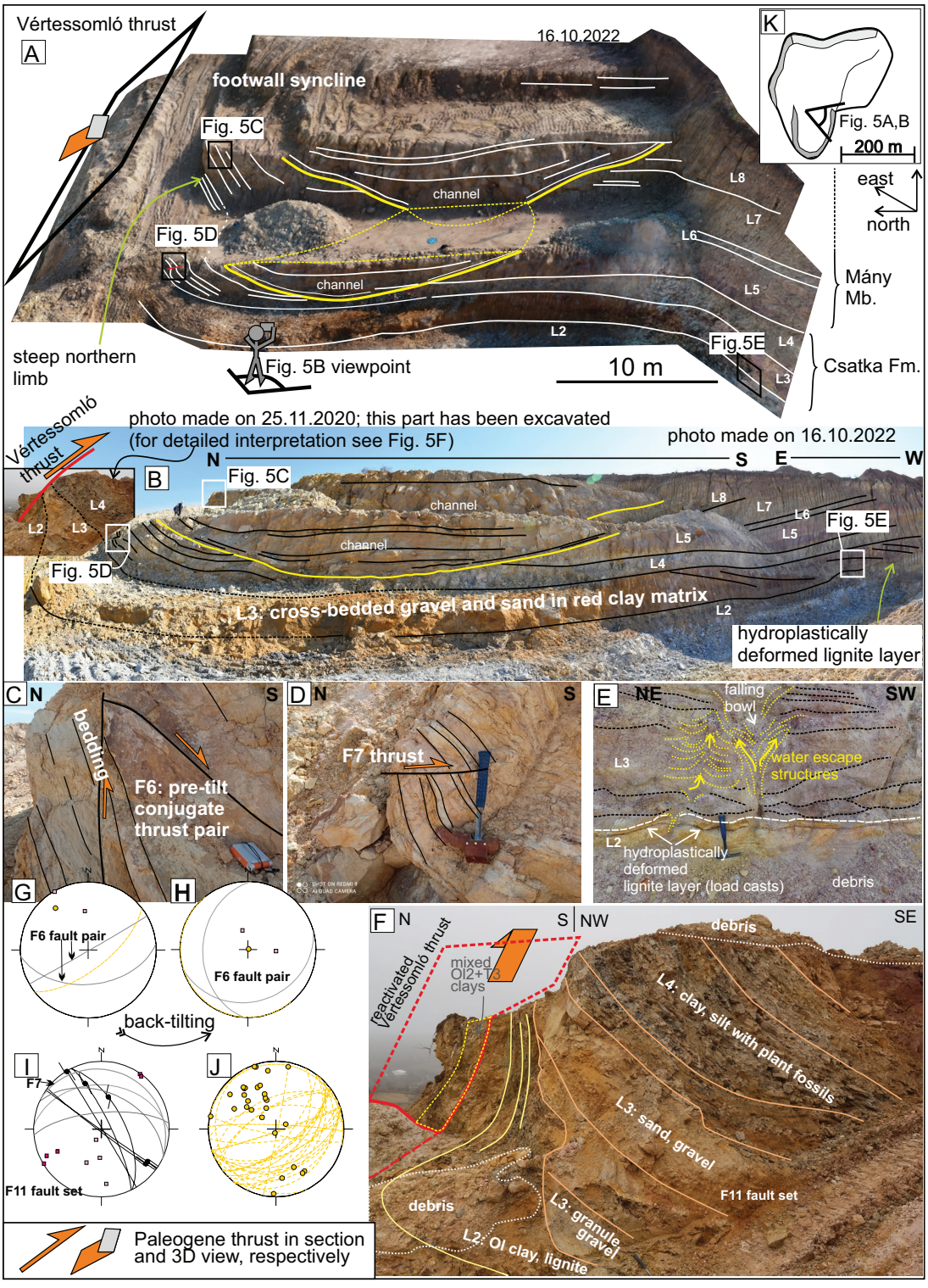

Fig. 5. Structures of the southern part of the eastern quarry wall of Strázsa Hill: **A** — interpreted 3D model of the Oligocene succession (for location of the viewpoint see Fig. 3A, Fig. 4A and Fig. 5K); **B** — interpreted photo of the southern part of the eastern wall: the beds of the Mány Mb. are folded into an asymmetrical footwall syncline in the front of the Vértessomló thrust (for location of the viewpoint see Fig. 3A, Fig. 4A and Fig. 5K); **C** — tilted conjugate thrust faults (F6) on the steeply south dipping beds of the Mány Mb. (for location see Fig. 5A, B); **D** — south-vergent thrust (F7) on the moderately south dipping beds of the Mány Mb. (for location see Fig. 5A, B); **E** — load casts and dewatering structures in the Mány Mb. (for location of the photo see Fig. 5A, B); **F** — photo of the already exploited lower part of the Oligocene succession on the vertical to overturned limb of the footwall syncline; note the thinning and onlapping of the beds on the flank of the syncline indicating syn-sedimentary folding (for location see Fig. 5B); **G** — present-day and **H** — back-tilted stereographic projection of the F6 fault pair; **I** — stereoplot of F7 and F11 fault sets; **J** — stereoplots of folded Oligocene beds (for legend of the stereoplots see Fig. 3B); **K** — point of view of Fig. 5A and B on the simplified map of the quarry.

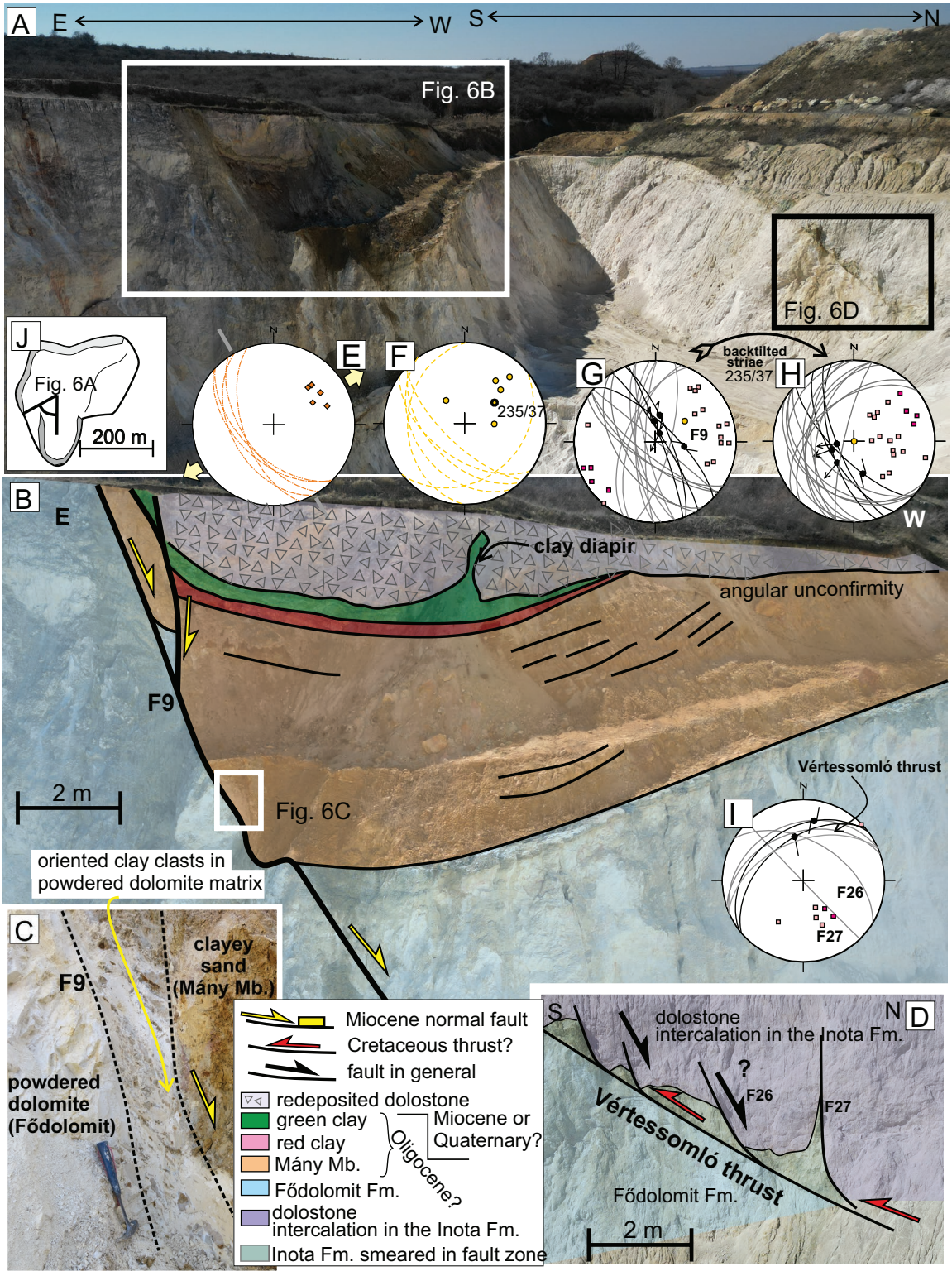

Fig. 6. Structures of the southern part of the western quarry wall (for location of the viewpoint see Fig. 3A, Fig. 6J): **A** — uninterpreted UAV photo of the southern part of the western wall; **B** — interpreted photos of the F9 fault (for location see Fig. 6A); **C** — zoomed in photo of the F9 fault core (for location see Fig. 6B); **D** — deformed Inota Fm. just above the Vértessomló thrust (for location see Fig. 6A); **E** — stereographic projection of deformation bands; **F** — projection of Oligocene beds dragged by the F9 normal fault; **G** — present-day and **H** — back-tilted stereographic projection of synthetic and antithetic faults measured in the F9 fault zone; the faults were back-tilted with the dip of the dragged Oligocene strata; **I** — projection of the Vértessomló thrust and F26-F27 faults (for legend of the stereoplots see Fig. 3B); **J** — point of view of Fig. 6A on the simplified map of the quarry.

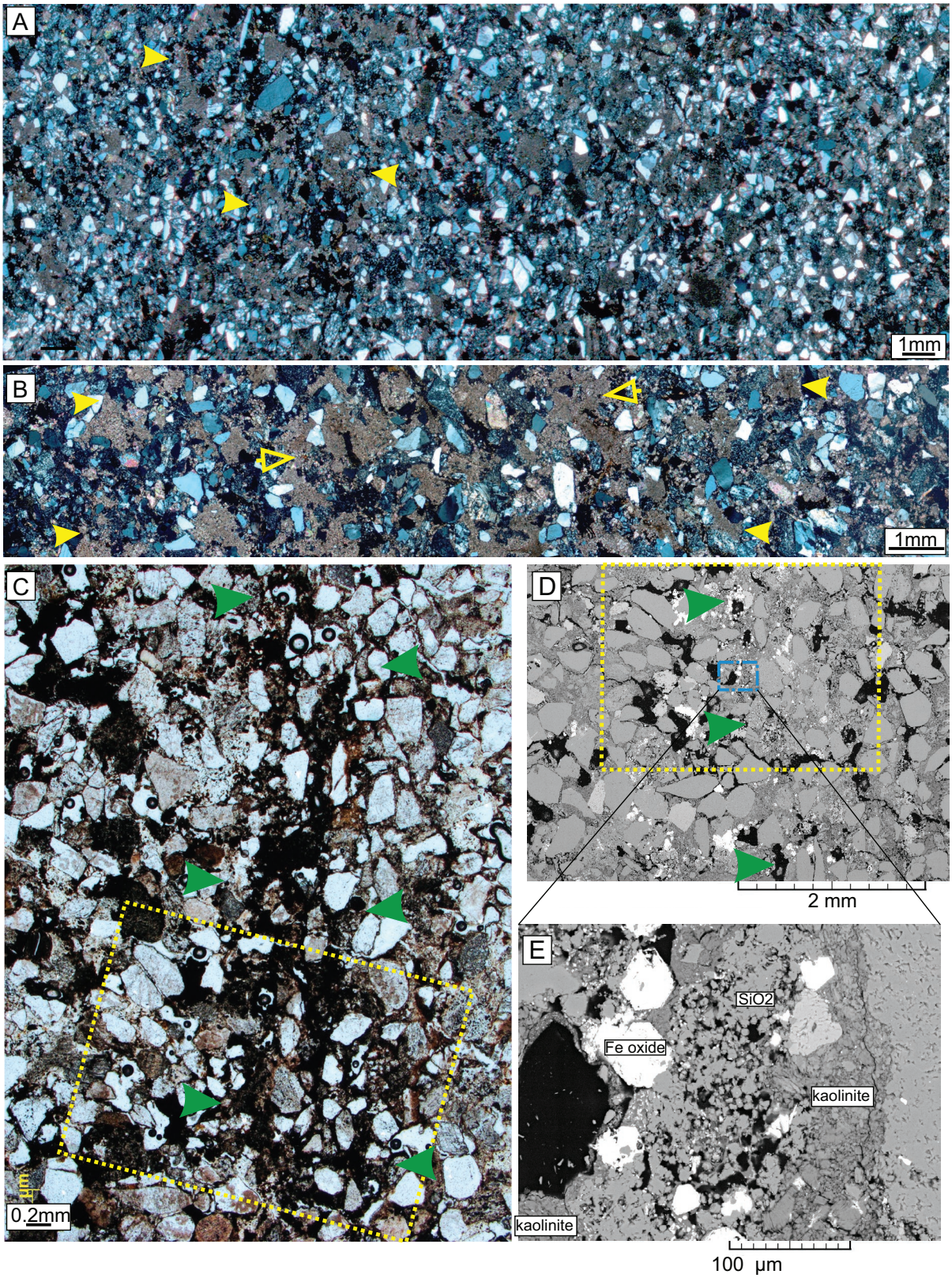

Fig. 7. Deformation bands in the southern part of the western quarry wall, near the F9 fault. **A, B** — Dilatation band in sample Zsam20-14a: yellow arrow indicates increased amount of fine-grained calcite in pores compared to host sandstone; B — yellow blank arrow indicates even more oversized pores filled with fine-crystalline calcite. **C** — The disaggregation band in sample Zsam20-14b, marked by the green arrow, shows granular flow without grain breakage. The pores are filled with kaolinite. Yellow inset shows the same areas in the pictures C and D. **D** — SEM BSE image of disaggregation band in the sandstone. Blue inset shows a closer view of the deformation band boundary. **E** — Along the band, silica (chalcedony?) and ferruginous minerals were precipitated, resulting in a dark brownish band boundary.

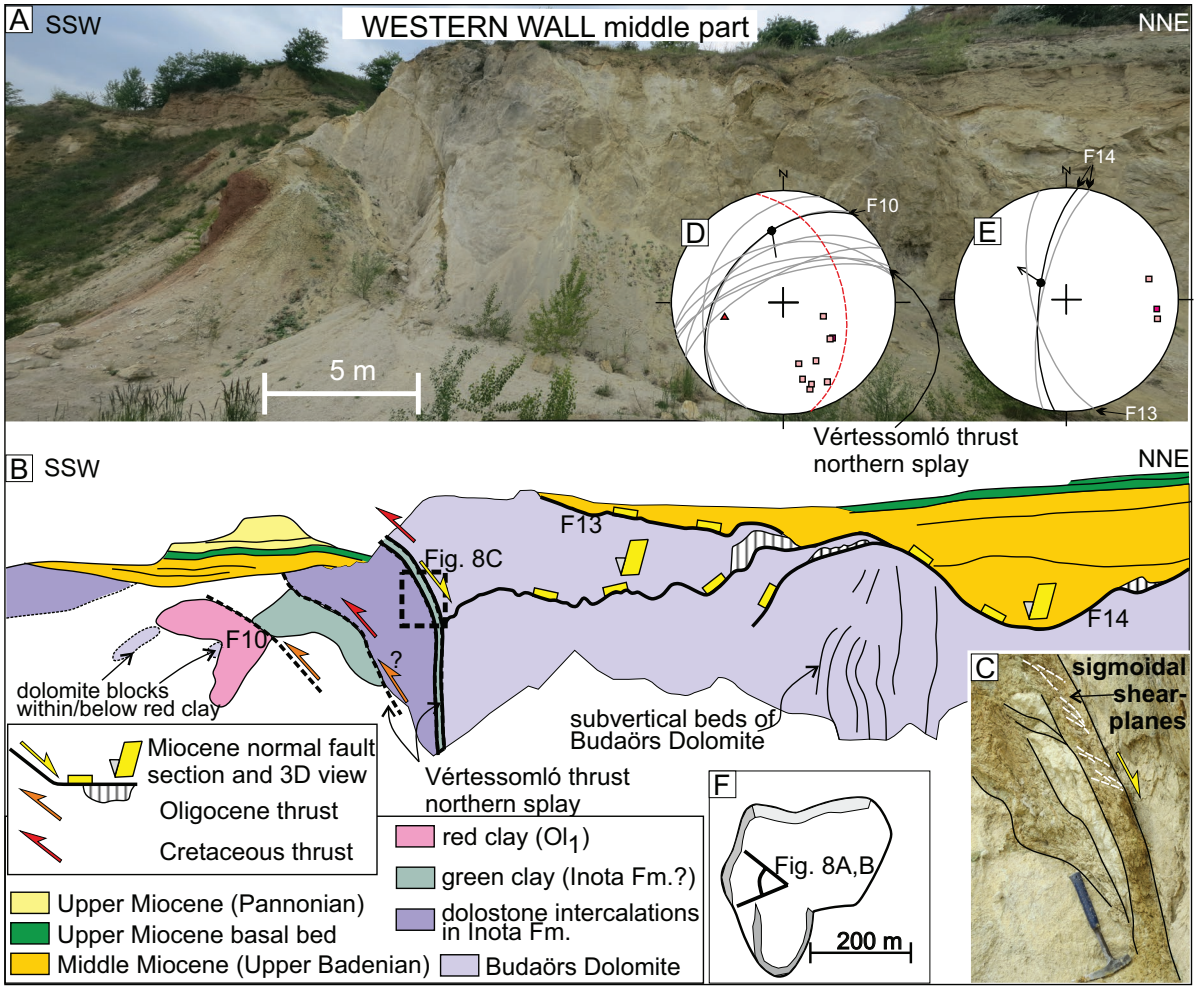

Fig. 8. Structures of the middle part of the western quarry wall (for location of the viewpoint see Fig. 3A and Fig. 8F): **A** — uninterpreted photo and **B** — interpreted drawing of the outcrop; **C** — detail of the northern splay of the Vértessomló thrust core (for location see Fig. 8B); **D** — stereographic projection of the F10 and the northern splay of the Vértessomló thrust; **E** — projection of the F13 and F14 faults (for legend of the stereoplots see Fig. 3B); **F** — point of view of Fig. 8A and B on the simplified map of the quarry.

extension (Fig. 9F). Horizontal slickolites observed on the Upper Miocene basal bed also indicate generally NE–SW shortening (Fig. 9F).

The NNW–SSE striking, vertical F16 fault (Fig. 9B, C) dissects the Budaörs Dolomite Fm. and the lower portion of the Middle Miocene deposits. The displacement along the fault gradually decreases upward and is sealed by the overlying Middle Miocene strata (Fig. 9B), as previously noted by Kercsmár et al. (2020). The lower segment of the F16 fault is represented by a 5–10 cm wide tensional fracture within the dolostone, filled with dolostone clasts embedded in red clay matrix (Fig. 9C). This feature records the initial phase of fracturing during the Oligocene, while fault movement occurred during the early stage of Middle Miocene sedimentation.

Northern wall, western part

The Miocene deposits unconformably overlie the Budaörs Dolomite Fm. on the northern wall of the quarry (Figs. 9, 10). Several minor antithetic and synthetic normal faults occur within the footwall block of the F15 fault. On the western part of the northern wall, the Miocene succession is cut by two east-dipping, vertically segmented normal faults (F18 and F19 on Fig. 9B). An antithetic F20 fault is located in the hanging wall of the F19 fault (Fig. 9B). The dip and orientation of these faults were estimated (Fig. 9H), as the structures are exposed high on the quarry wall. The F18 fault shows upward-increasing displacement (Fig. 9B).

On the eastern part of the northern wall, several normal faults crosscut the base-Miocene horizon (F22, F23, and F25 on Fig. 10B). These structures could not be measured directly, as they are exposed high on the quarry wall. Based on our estimations, the faults dip towards the SW (Fig. 9C). The F22 and F23 normal faults are clearly sealed by the Upper Miocene basal bed, and the upper beds of the Middle Miocene succession also seal the faults (Fig. 10B). The underlying Middle Miocene (upper Badenian) deposits are thicker in the hanging wall of these faults than in the footwall. In the hanging wall of

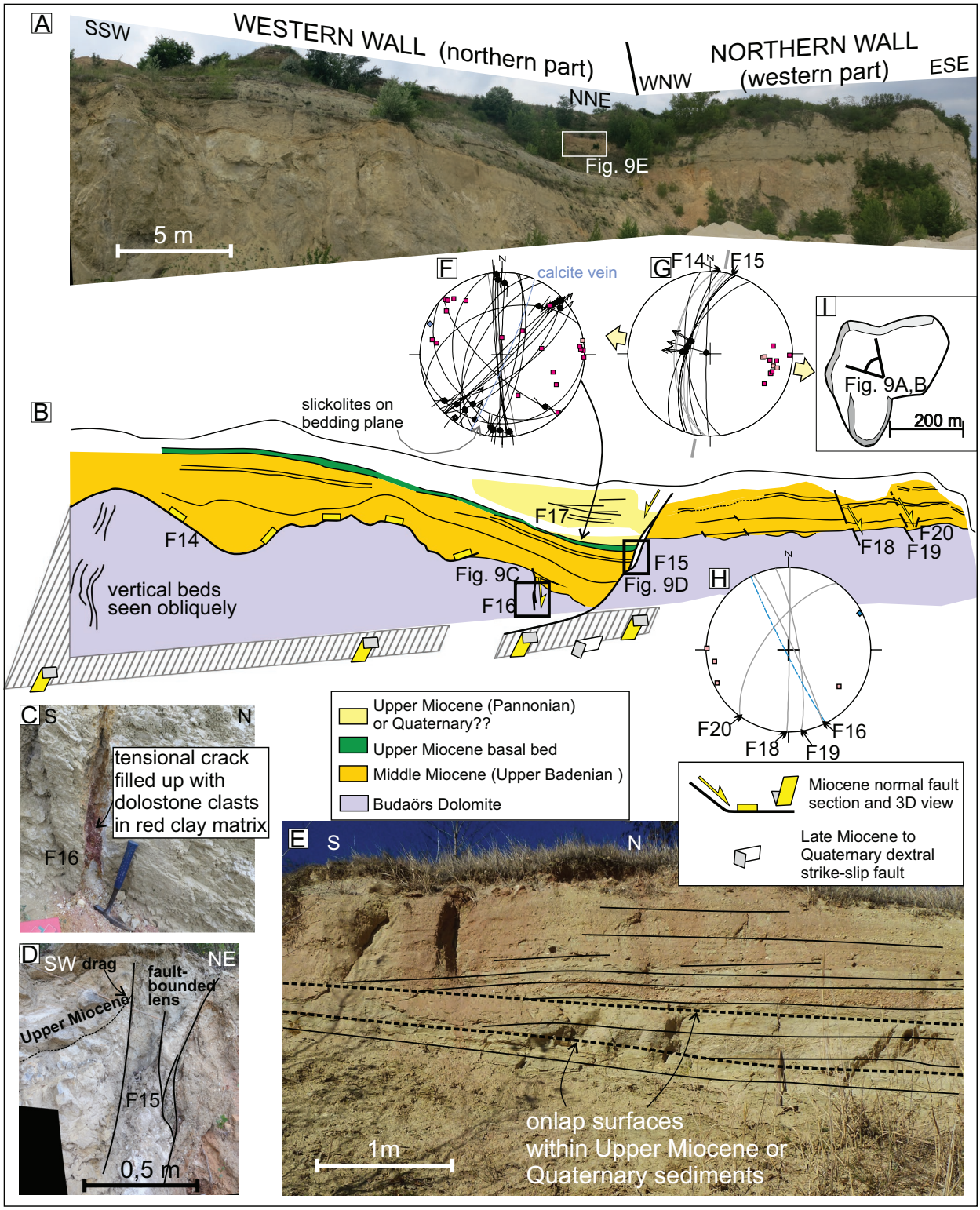

Fig. 9. Structures of the northwestern corner of the quarry (for location of the viewpoint see Fig. 3A and Fig. 9I): **A** — uninterpreted and **B** — interpreted photos of the outcrop; **C** — detail of the F16 tensional crack (for location see Fig. 9B); **D** — detail of the F15 fault core (for location see Fig. 9B); **E** — silty sand with redeposited dolostone breccia with uncertain Upper Miocene or Quaternary age; note the onlap surfaces within the succession (for location see Fig. 9A); **F** — stereographic projection of the F17 fault set; **G** — stereographic projection of fault-slip data measured in the F14 and F15 fault-zones; **H** — stereographic projection of the F16, F18, F19 and F20 faults (for legend of the stereoplots see Fig. 3B); **I** — point of view of Fig. 9A and B on the simplified map of the quarry.

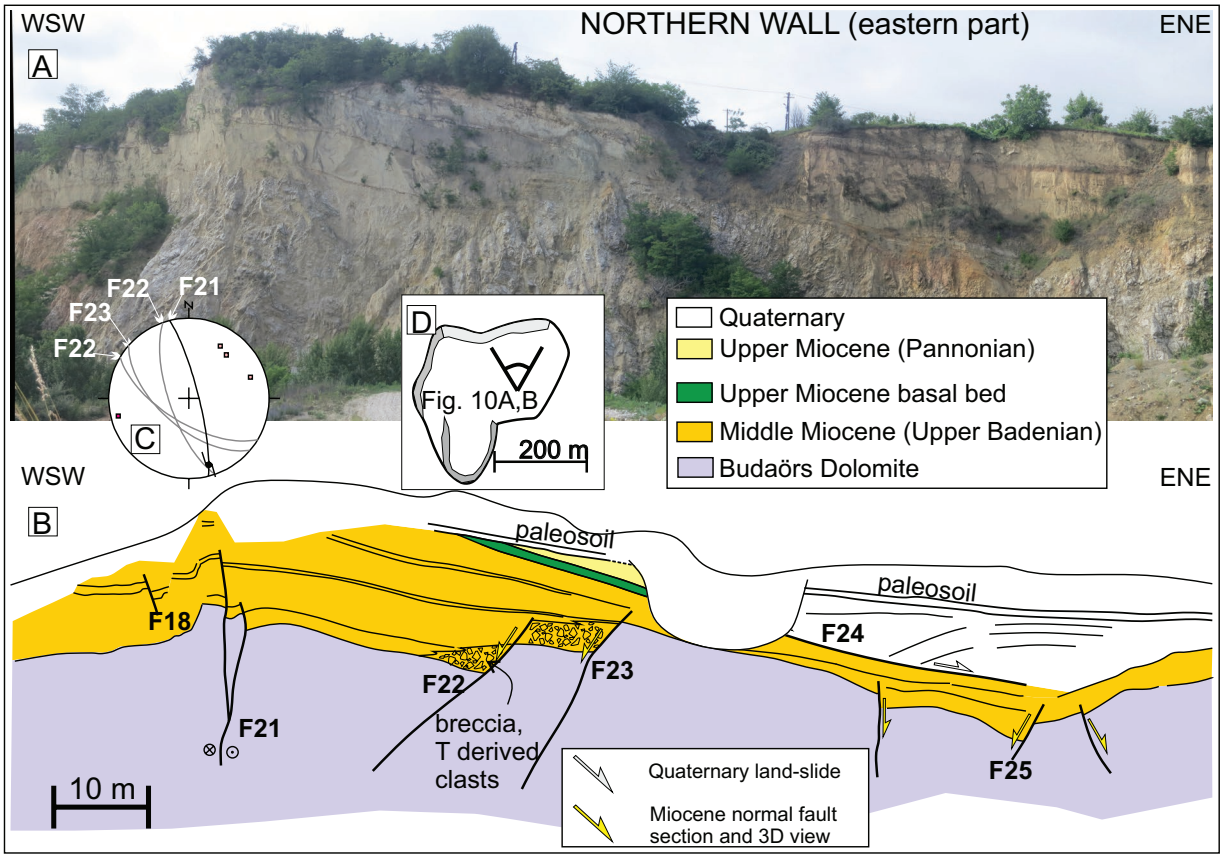

Fig. 10. Structures of the eastern part of the northern quarry wall (for location of the viewpoint see Fig. 3A and Fig. 10D): **A** — uninterpreted photo and **B** — interpreted profile of the outcrop; **C** — projection of the F21, F22, and F23 faults (for legend of the stereoplots see Fig. 3B); **D** — point of view of Fig. 10A, B on the simplified map of the quarry.

the F22 and F23 normal faults, the Middle Miocene sand interfingers with breccia wedges composed of redeposited Triassic dolostone clasts (Fig. 10B). The breccia bodies taper and wedge out away from the faults. The subvertical F21 fault crosscuts the Miocene beds. In the lower part, subhorizontal slickenlines plunge southward, indicating a poorly constrained dextral slip (Fig. 10B, C).

Towards the easternmost part of the northern wall, the Upper Miocene succession is laterally replaced by Quaternary deposits (Fig. 10B). The Quaternary strata display a roll-over geometry in the hanging wall of a gently dipping surface (F24), which is sealed by a dark paleo-soil layer (Fig. 10B). This surface is tentatively interpreted as a Quaternary slide plane formed by slope processes.

Discussion: Paleostress analysis and geodynamic background of the deformation phases

D1 – Triassic NE–SW extension

The Middle Triassic represents the main period of extensional tectonics within the TR (Budai & Vörös 1993, 2006), associated with the regional rifting and spreading of the Neotethys Ocean (Csontos & Vörös 2004; Gawlick et al. 2021). Late Triassic extension is well documented in the southwestern part of the TR and is interpreted as the result of continental rifting related to the opening of the Alpine Tethys (Budai et al. 1999; Héja et al. 2018). Despite the contrasting facies and depositional environments reported from different parts of the range (Budai et al. 1999; Budai & Vörös 2006; Karádi et al. 2022), direct field evidence for Triassic normal faulting is scarce. The few documented cases comprise Middle Triassic faults from the central TR (Budai & Vörös 2006; Csicsek & Fodor 2016; Fodor et al. 2017) and Norian–Rhaetian faults and grabens in the southwestern TR (Héja et al. 2018).

In the present study, we identified Carnian normal faults (F1 fault) and associated gravitational slide planes (D1 phase). Although these faults lack striae, their dip direction indicates NE–SW extension (Figs. 4I, 11L), consistent with other Late Triassic and Jurassic structural data from the TR (Fodor 2008; Csicsek & Fodor 2016; Héja et al. 2018). This Carnian extension likely contributed to the formation of the intraplatform basins in the northeastern TR that persisted throughout the Late Triassic, such as the Mátyáshegy Basin in the Buda Hills

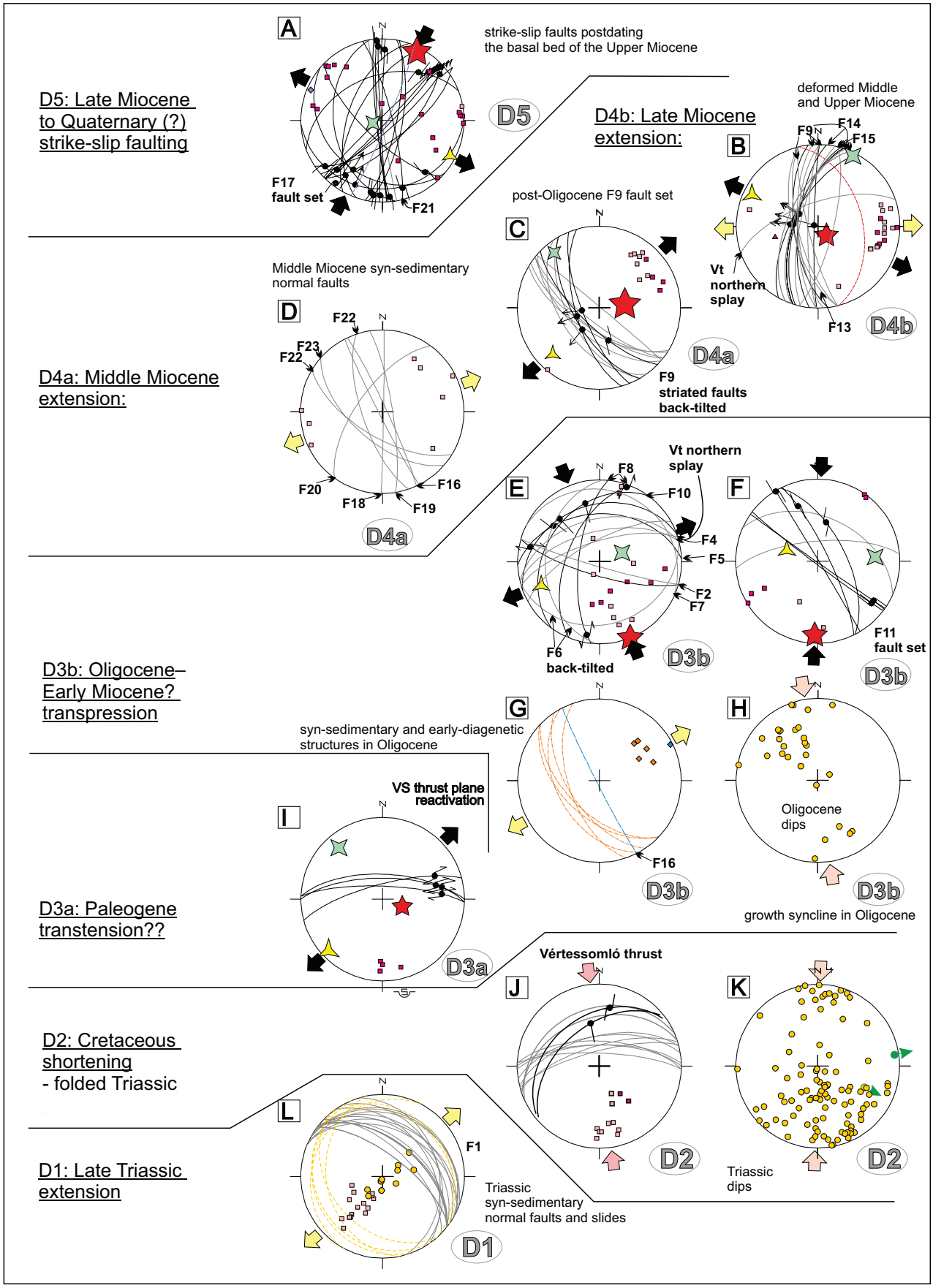
D5: Late Miocene to Quaternary (?) strike-slip faulting
A
strike-slip faults postdating the basal bed of the Upper Miocene
F17 fault set
F21
D5
D4b: Late Miocene extension:
deformed Middle and Upper Miocene
B
F9
F14
F15
Vt northern splay
F13
D4b
post-Oligocene F9 fault set
C
D4a
F9 striated faults back-tilted
D4a: Middle Miocene extension:
Middle Miocene syn-sedimentary normal faults
D
F22
F23
F22
F20
F18
F19
F16
D4a
Vt northern splay
E
F8
F10
F4
F5
F2
F7
F6 back-tilted
D3b
F
F11 fault set
D3b
D3b: Oligocene–Early Miocene? transpression
G
F16
D3b
syn-sedimentary and early-diagenetic structures in Oligocene
H
Oligocene dips
D3b
growth syncline in Oligocene
VS thrust plane reactivation
I
D3a
D3a: Paleogene transtension??
Vértessomló thrust
J
D2
K
D2
Triassic dips
D2: Cretaceous shortening
- folded Triassic
L
F1
D1
Triassic syn-sedimentary normal faults and slides
D1: Late Triassic extension

Fig. 11. Fault-slip analysis of measured structures of Strázsa Hill: **A** — faults of the Late Miocene to Quaternary(?) strike-slip faulting (D5); **B** — N–S striking Miocene normal faults (D4b sub-phase); **C** — back-tilted faults within the F9 fault-zone indicate NE–SW extension (D4a sub-phase); **D** — Middle Miocene syn-sedimentary normal faults (D4a sub-phase); **E** — transpressional structures of the quarry indicate NNW–SSE compression and ENE–WSW extension; these structures deform the Oligocene succession, but pre-date the Middle Miocene (D3b sub-phase); **F** — dextral strike-slip faults and oblique dextral thrusts measured on Oligocene formations in the front of the Vértessomló thrust indicate N–S compression (D3b); **G** — sediment-filled tension crack and deformation bands show syn-sedimentary and early diagenetic NE–SW extension for the Oligocene (D3b); **H** — bedding dips of Oligocene strata outlines a footwall syncline in the front of the Vértessomló thrust (D3b); **I** — oblique dextral-normal reactivation of the Vértessomló thrust (D3a sub-phase); **J** — the D2 Vértessomló thrust (D2); **K** — folded Triassic dip data (D2); **L** — Late Triassic D1 syn-sedimentary normal faults indicate NE–SW extension (D1), (for legend of the stereoplots see Fig. 3B).

and the Csővár Basin (for location see Fig. 2A) (Haas & Budai 2014).

The broader geodynamic context of this Late Triassic extension remains uncertain. During the Carnian, the TR was located on the passive margin of the Neotethys, where rifting related to its opening should theoretically have already ceased by that time on the Adriatic continental margin. Therefore, the observed early extensional deformation may be linked to gravitational gliding along the passive margin. Alternatively, it could represent an early, far-field response to the continental rifting of the Alpine Tethys, although the associated rift-related structures in the southwestern TR are somewhat younger – of middle Norian–Rhaetian age (Héja et al. 2018).

D2 – Cretaceous N–S shortening and the formation of the Vértessomló thrust

Style of deformation: imbrication vs. gentle folding

Structural data from Strázsa Hill indicate that the major tilting and folding of the Triassic beds occurred along the Vértessomló Thrust, which is prominently exposed in the eastern wall of the quarry (Fig. 4). Both map-scale observations (Héja et al. 2022) and fault-slip analysis suggest an overall E–W to ENE–WSW strike of the thrust (Figs. 3, 11J). Despite the significant variation in bedding dip directions, a N–S striking best-fit great circle can be plotted through the poles of the Triassic strata at Strázsa Hill (Fig. 11K). The observed scatter is partly attributed to local folds with vertical axes that were formed within shear zones. The E–W-trend of fold axes is consistent with the orientation of the map-scale, south-vergent Vértessomló thrust (Fig. 11J) (Héja et al. 2022).

The main Vértessomló thrust exhibits an intermediate décollement within the incompetent Inota Fm., as indicated by the exposed beds of the formation that are parallel to the thrust surface (Fig. 4B) and define a hanging wall flat. The cut-off angle between the main thrust and the beds of the Fődolomit Fm. in the footwall is approximately 30°, forming a well-developed footwall ramp. Additionally, unexposed south-vergent thrusts are inferred south of the quarry and are proposed to be responsible for the northward tilt of the footwall of the Vértessomló thrust (Héja et al. 2022). This deformation likely resulted in the steepening of both the thrust surface itself (up to 50–60°) and its footwall, where the Fődolomit Fm. dips northwards at 20–30° (Fig. 4B). According to Héja et al. (2022), the Vértessomló thrust and the adjacent structures form a south-vergent imbricate thrust system above a shallow detachment horizon located within the Middle Triassic succession. This imbrication of the Triassic sequence represents an important new interpretation of regional geology, as earlier models primarily invoked Cenozoic strike-slip faults to explain the map-view repetition of different Mesozoic formations (Maros 1988; Balla & Dudko 1989).

These imbricates demonstrate a deformation style that differs from that of the western neighbouring region (Gerecse Hills) but closely resembles the eastern segment of the TR (Buda and Pilis Hills; Figs. 2A, 12). In the Gerecse Hills, only very gentle folds are present, characterised by large interlimb angles of 130–150° (Fig. 12; Sasvári 2008; Fodor et al. 2018). In contrast, E–W striking imbricates appear in the vicinity of the study area (Héja et al. 2022). Eastward, the imbricate system continues, as inferred from sparse structural observations and surface geological maps (Wein 1977; Fodor et al. 1994; Palotai et al. 2006). In the Buda and Pilis Hills, E–W- and NW–SE-striking faults define a more complex structural pattern (Fig. 12). This indicates a distinct change in structural style within the TR. We propose that this variation reflects differential Cretaceous shortening. The NE part of the TR likely experienced more intense local shortening than the central and western segments, as it was located closer to the active Neotethyan margin (Császár & Árgyelán 1994; Tari 1994; Palotai et al. 2006; Schmid et al. 2008; Sasvári 2009; Fodor et al. 2013).

The orientation of the main contractional structures becomes even more complex when the entire TR is considered (Fig. 12). The central part of the TR (Bakony) is dominated by a major NE–SW-trending syncline, parallel to the thrusts of the Balaton Highland (e.g., Litér thrust; Budai et al. 1999). In contrast, the Buda and Pilis Hills, in the easternmost part of the TR, are characterised by NW–SE-trending Cretaceous folds (Fig. 12) (Wein 1977; Balla & Dudko 1989; Fodor et al. 1994; Palotai et al. 2006). Early studies explained this change in structural trend by oroclinal bending (Wein 1977; Balla & Dudko 1989), implying that the south-vergent thrusts in the study area could represent the hinge zone of this orocline. Later investigations, however, largely following the pioneering work of Tari (1994), interpreted the variable structural orientations in the central and northeastern TR as a result of polyphase folding (Albert 2000; Kercsmár 2004; Pocsai & Csontos 2006; Sasvári 2008; Tari & Horváth 2010; Fodor et al. 2013, 2018; Szives et al.

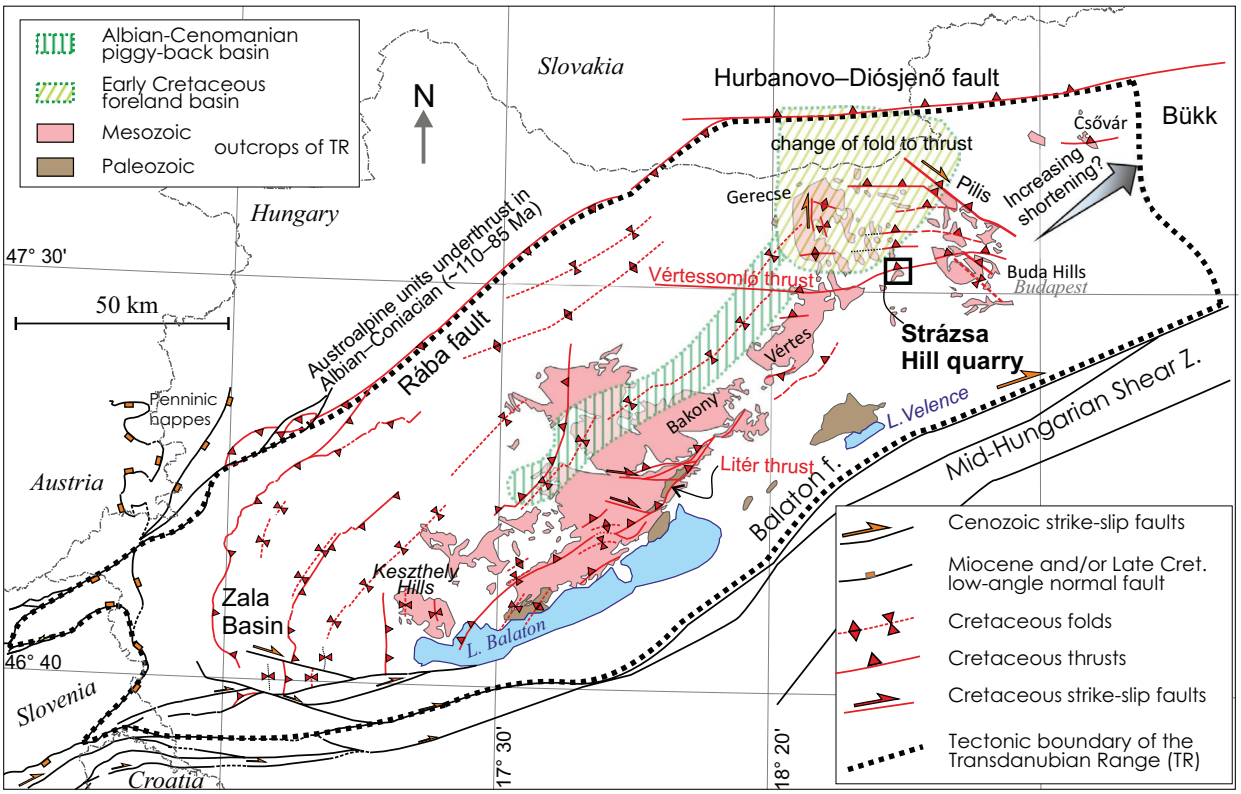

Fig. 12. Major structures of the Cretaceous fold and thrust belt of the TR (after Fodor et al. 2017, modified).

2018). The Gerecse Hills are likely the only area where all three structural orientations of folds and thrusts coexist (Fodor et al. 2018), whereas only one shortening direction is evident in the current study area. This implies that the northern part of the TR underwent a spatially and/or temporally variable contraction. Resolving this issue critically depends on the precise timing of these structures (see below).

Age of deformation, comparison with structural data of the other parts of the TR

Although Oligocene beds are deformed by the Vértessomló thrust (Fig. 5), our observations at Strázsa Hill suggest that the amount of syn- and post-Oligocene shortening does not exceed a few tens of meters. In contrast, thrusting of the Budaörs and Inota fms. over the Fődolomit Fm. indicates displacement exceeding one kilometre along the thrust before Oligocene sedimentation. Borehole data from the surrounding area reveal that Middle Eocene layers also unconformably overlie the folded Triassic succession (Héja et al. 2022), implying that major thrusting along the Vértessomló thrust occurred before the Middle Eocene. Nevertheless, this still represents a broad time window for the contractional deformation. To further constrain the timing of the local D2 phase, we compare our structural observations with data from other regions of the TR, where in some places a more complete Cretaceous succession is preserved (Fig. 12).

The earliest far-field sign of orogenic activity within the TR is represented by the formation of the Lower Cretaceous Gerecse foreland basin (Császár & Árgyelán 1994; Tari 1994) (Fig. 12). Because Early Cretaceous facies boundaries trend NW–SE (Tari 1994; Császár 1995), most authors associate the NW–SE–striking pre-Eocene folds and thrusts of the northeastern Transdanubian Range with the development of this foreland basin (Tari 1994). Palotai et al. (2006), however, did not exclude the possibility that thrusting had already initiated during the Late Jurassic in the Pilis Hills. The deformation prograded from NE to SW (Csontos & Vörös 2004; Sasvári 2008; Tari & Horváth 2010; Fodor et al. 2013, 2018; Szives et al. 2018). Based on facies distribution, Tari (1994) proposed that the orogenic front related to NE–SW shortening reached the TR in the Aptian. Sasvári (2008, 2009) assigned the Aptian age to some folds in the Gerecse Hills, whereas Pocsai & Csontos (2006) suggested Barremian to Aptian syn-sedimentary deformation along some thrusts within the TR, including the Vértessomló thrust. Szives et al. (2018) further constrained the timing of deformation to the late Aptian (~116–113 Ma), assuming that thrusting postdates sedimentation in the Lower Cretacous Gerecse foreland basin but predates the formation of the NE–SW-trending major syncline in the central TR. If the E–W and NW–SE-striking folds and thrusts were approximately coeval, they must have developed within a heterogeneous deformation field.

The NE–SW-trending major syncline of the central TR (Fig. 12) began forming in the Early Albian, as evidenced by the involvement of the Aptian to lowest Albian Tata Limestone in folding, which is unconformably overlain by Middle Albian deposits (Fodor et al. 2017). Tari (1994) and Tari & Horváth (2010) also attributed an Albian age to these major fold structures. Folding of this NE–SW-trending syncline continued during and after the deposition of Albian-Cenomanian sediments (Fig. 12) (Tari 1994; Héja 2015). In the southwestern part of the TR, Upper Cretaceous Santonian–Campanian Gosau-type deposits unconformably overlie folds and thrusts, indicating the termination of contractional deformation (Haas et al. 1984; Fodor et al. 2017). Nevertheless, the spatial distribution of Upper Cretaceous basins and platforms – aligned parallel to thrusts – suggests that compressional tectonics persisted locally during Late Cretaceous sedimentation (Tari 1994). Kercsmár (2004) further associates the formation of pre-Eocene red calcite dykes, in connection with Upper Cretaceous Sukoró Lamprophyre Fm., with this deformation phase.

Based on the pre-Cenozoic map of Haas et al. (2010), the Vértessomló thrust obliquely cuts the main syncline of the central TR (Fig. 12). However, Fodor et al. (2013, 2018) interpret these two structures as coeval. This interpretation is based on fault-slip data indicating dextral-reverse slip on the western segment of the Vértessomló thrust (Fodor 2008), and on the observation that the thrust postdates the Lower Albian deposits in the Vértes Hills (Császár 1995).

In the north-easternmost part of the TR, local evidence does not exclude a younger age for major N–S shortening, potentially extending into the Late Cretaceous or even early Paleocene. In the Csővár area (Fig. 12), thin slices of Upper Cretaceous deposits are tectonically intercalated between south-vergent thrust sheets composed of Triassic carbonates. These structures are overlain by Upper Eocene strata (Haas et al. 1997; Benkő & Fodor 2002). In conclusion, the age of the Vértessomló thrust remains debated: it may have formed during the Aptian or Albian, but subsequent reactivations could have occurred later, possibly in the Late Cretaceous or even earliest Paleogene.

Geodynamic background of the Cretaceous deformations

The TR was located at the junction of the Alpine–Carpathian–Dinaridic orogenic system before the Cenozoic eastward extrusion of the Alcapa block (Schmid et al. 2008). Consequently, its structural evolution can be interpreted within the framework of the development of these three orogenic systems. Most authors associate the Early Cretaceous Gerecse foreland basin and the related NW–SE-trending folds and thrusts of the northeastern TR with the subduction and obduction of the Neotethys Ocean (Császár & Árgyelán 1994; Tari 1994). Specifically, this basin is thought to have formed at the front of the obducted Neotethyan ophiolites, which are widespread in the Dinarides (Pocsai & Csontos 2006; Fodor et al. 2013; Szives et al. 2018). From this "Dinaric" perspective, the TR occupied a lower-plate position relative to the obducted ophiolites during the Early Cretaceous.

The formation of the major syncline in the central TR and the SE-directed thrusts of the Balaton Highland (e.g., the Litér Thrust) is commonly linked to the Eoalpine or Austroalpine orogeny (Tari 1994; Fodor et al. 2017, 2018; Szives et al. 2018), which resulted from intracontinental subduction within the Adriatic Plate (Stüwe & Schuster 2010). From an Eastern Alpine perspective, the TR can be correlated with the Drauzug–Gurktal nappe system of the Eastern Alps (Schmid et al. 2008), representing the uppermost thick-skinned nappe of this orogenic system and occupying an upper-plate position relative to the Austroalpine HP belt (Tari 1994; Tari & Horváth 2010; Fodor et al. 2013, 2018). According to Szives et al. (2018), the TR shifted from a lower-plate to an upper-plate position around the Aptian–Albian boundary.

From a Western Carpathian perspective, however, a somewhat different tectonic evolution has been proposed. Plašienka (2018) interpreted the SW–S-vergent thrusts of the northeastern TR together with the SE-directed thrusts of the Balaton Highland as forming part of a south-vergent, Late Jurassic–mid-Cretaceous retrowedge of the Carpathian orogen. This system was developed following the late Middle Jurassic subduction and closure of the Meliata branch of the Neotethys. A broadly similar interpretation was suggested by Benkő & Fodor (2002) for the south-vergent thrusts in the Csővár area, although they proposed a slightly younger, Late Cretaceous timing.

In summary, both the geodynamic setting and the timing constraints of the Vértessomló thrust remain debated. It may have formed either as a result of obduction-related processes or during deformation associated with the Austroalpine orogeny.

D3 – Paleogene strike-slip faulting, oblique reactivations of the Vértessomló thrust

Middle Eocene dextral-normal reactivation of the Vértessomló thrust (D3a sub-phase)

Although Eocene deposits are absent at Strázsa Hill, borehole data from immediately north of the quarry reveal a thick Middle Eocene succession (Héja et al. 2022). The southern boundary fault of this Middle Eocene basin is the E–W-striking Környe–Zsámbék fault (Fig. 2B) (Véghné Neubrandt et al. 1978; Balla & Dudko 1989; Kercsmár 2005; Kercsmár et al. 2006), which runs parallel to, and partly reactivates, the Cretaceous Vértessomló thrust (Fig. 2B, Héja et al. 2022). Cross-section data indicate that the Middle Eocene deposits form a half-graben geometry in the hanging wall of the Környe–Zsámbék fault (Héja et al. 2022). Fault-slip measurements suggest that this structure accommodated a dextral-normal fault motion during the Middle Eocene.

Dextral-normal slickenside lineations observed on the Vértessomló thrust (sub-phase D3a) indicate its reactivation under an NNE–SSW extensional stress field (Fig. 11I). This

deformation post-dated the D2 thrusting phase, although its exact relationship to the subsequent Oligocene–Miocene thrusting remains uncertain. The transtensional reactivation on the Vértessomló thrust could be associated with the above-described Middle Eocene transtensional tectonic regime, but a younger, Miocene reactivation event cannot be excluded (see below).

Structural and sedimentological evidence for Oligocene syn-sedimentary folding (D3b sub-phase)

Oligocene beds unconformably overlie the Vértessomló thrust and the tilted Triassic succession. However, the distribution and internal geometry of the Oligocene strata indicate a mild reactivation of the Vértessomló thrust during their deposition. In the southern part of the eastern quarry wall, Oligocene beds are folded into an asymmetric footwall syncline in the front of the thrust, implying, based on fault-slip data (see below), a dextral-reverse reactivation of the structure (Fig. 5A, B, F). The structural contact between the Triassic and Oligocene strata in the western wall further indicates the reactivation of the northern splay of the Vértessomló thrust (Fig. 8B). Middle Miocene deposits unconformably cover both the footwall and the hanging wall of this splay, suggesting that the dextral-reverse reactivation occurred before Middle Miocene sedimentation. Several sedimentological and structural features indicate that this folding was coeval with Oligocene deposits. The Oligocene beds thicken towards the core of the footwall syncline associated with the Vértessomló thrust (Fig. 5A, B), while coarse-grained Oligocene strata thin and onlap onto its overturned limb (Fig. 5F). These relationships define a growth-syncline geometry, characteristic of syn-sedimentary folding (Fig. 13B) (Ford et al. 1997; Ortner et al. 2016).

Sedimentary evidence also supports the reactivation of the Vértessomló thrust. The red clay at the Oligocene succession occurs exclusively above the middle thrust sheet, composed predominantly of the Inota Fm., situated between the two splays of the Vértessomló thrust (Figs. 3A, 4B, 8B, 13A). We propose that the denuded surface of the middle thrust sheet formed a shallow topographic depression relative to the lower and upper thrust sheets, owing to the mechanically weak lithology of the Inota Fm. This depression likely controlled the accumulation of the red clay (Fig. 13A). According to Szabó & Ravasz (1970), the bauxites and kaolinites of the TR originated from the surface weathering of Middle Triassic pyroclastic rocks under subtropical climate conditions. Because these Middle Triassic tuffitic clays are compositionally similar to the Inota Fm. (Budai et al. 2015), so it cannot be ruled out that the kaolin-rich red clays exposed in the quarry formed through subaerial weathering of the Inota Fm. itself.

The red clay is preserved only within sedimentary dykes in the hanging wall of the northern splay of the Vértessomló thrust, where the Miocene succession directly overlies the Budaörs Dolomite Fm. (F16 on Figs. 9C, 13A). In contrast, the red clay is absent at the base of the Oligocene succession in the footwall of the Vértessomló thrust (lower thrust sheet, consisting of Fődolomit Fm.). Nevertheless, Triassic clasts and redeposited red clay horizons appear in the upper part of the Oligocene section within the footwall of the Vértessomló thrust (Fig. 5B). We interpret these redeposited sediments as derived from the hanging wall of the Vértessomló thrust, specifically from the middle and upper thrust sheets (Fig. 13B). The steep cross-bedding observed in the Oligocene clastics in the southern part of the eastern quarry wall (Fig. 5B) indicates a high-energy terrestrial sedimentary environment characterised by short transport distances and rapid sediment deposition (Fig. 13B). The underlying coaly-clay layer was hydroplastically deformed under the load of the rapidly deposited sediments. Compaction features and dewatering structures in the coarse-grained sediment (Figs. 5E, 13B) further indicate both sediment loading and tectonic pressure. The Oligocene tidal channel geometry also appears to have been influenced by the Vértessomló thrust, to which it is aligned subparallel (Fig. 5A). We therefore interpret all these sedimentary and structural features as evidence of dextral-reverse reactivation of the Vértessomló thrust during the Oligocene (Fig. 13B).

Fault-slip data of Oligocene structures (D3b sub-phase)

The folding of the Oligocene strata immediately below the Vértessomló thrust indicates N–S-oriented shortening (Fig. 11H), whereas the associated striated faults are more consistent with a strike-slip regime (Fig. 11E, F). Most of the faults measured within the Oligocene succession record NW–SE or N–S compression accompanied by perpendicular extension (Fig. 11E, F). Similar strike-slip stress fields have been reported for the Eocene to Early Miocene of the northern TR by several authors (Fodor et al. 1992, 2018; Kercsmár 1993, 2005; Bada et al. 1996; Kercsmár et al. 2006; Fodor 2008, 2010). These studies inferred the maximum principal stress axis (σ1) oriented between WNW–ESE to NNW–SSE.

Minor thrusts and strike-slip faults (e.g., F7 on Fig. 5D) overprint the Oligocene sequence, whereas the Miocene deposits appear undeformed by this phase of deformation. Tilted thrusts (F6 fault set on Fig. 5C), which crosscut Oligocene beds in the northern limb of the footwall syncline of the Vértessomló thrust, indicate that NW–SE shortening was already active during the initial folding of the Oligocene succession (Fig. 5G, H). The sediment-filled tension crack along the F16 fault (Fig. 9C) indicates NE–SW extension of Oligocene age (Fig. 11G). Dilation and disaggregation deformation bands in the SW corner of the quarry (Figs. 5, 6, 11G) suggest deformation of unconsolidated sediments. Disaggregation bands typically form fat depths of <200 m, whereas dilation bands develop even shallower (Beke et al. 2019). Host rock rheology progressively changed due to concurrent cementation, which finally prevented non-destructive deformation mechanisms. Deformation and cementation seem to be aligned processes and are likely to have happened during the early part of the Late Oligocene sedimentation before the deposition of the complete 300–400 m thick succession.

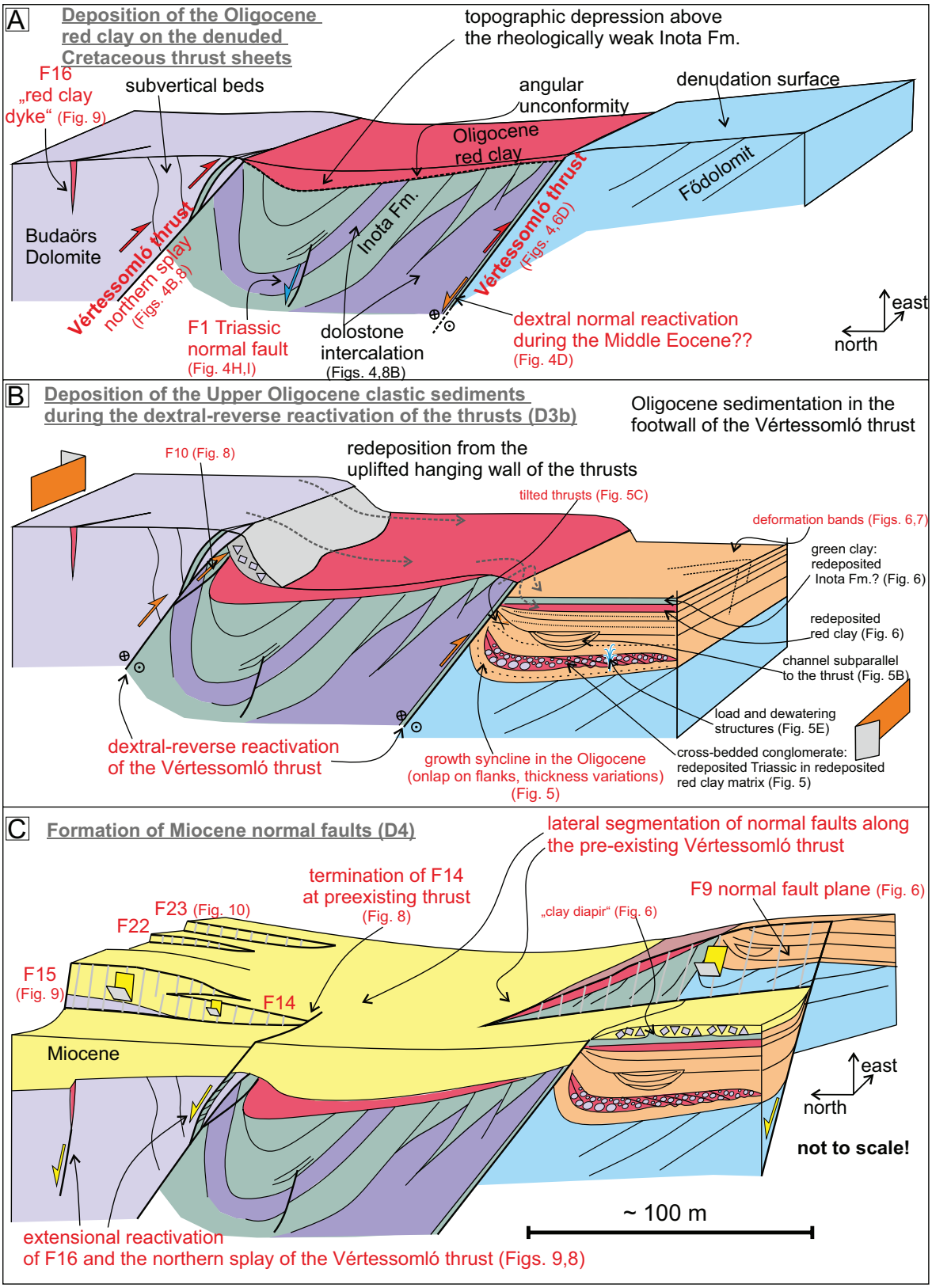

Fig. 13. Schematic 3D model for the structural evolution of Strázsa Hill: **A** — formation of the D2 Vértessomló thrust and the denudation of the tilted Triassic rocks; **B** — the deposition of the Mány Mb was controlled by the dextral-reverse reactivation of the Vértessomló thrust (D3b), consequently, the hanging wall of the thrust was an area of erosion and/ or non-deposition during the Oligocene; **C** — formation of west- and southwest-dipping normal faults during the deposition of the Miocene succession (D5).

Although these syn-sedimentary and early diagenetic structures record NE–SW extension (Fig. 11G), we interpret them as coeval with the folding of the Oligocene beds in the footwall of the Vértessomló thrust. The coexistence of extensional and compressional structures indicates a strike-slip (transpressional) stress regime during the Oligocene. Fault-slip data (Fig. 11E, G) further confirm the Oligocene displacement along the Vértessomló thrust was not purely dip-slip but involved dextral-reverse reactivation.

Paleogene structures and the Hungarian Paleogene retroarc foreland basin

According to the model of Tari et al. (1993), Paleogene sedimentation of the TR took place within a retroarc foreland basin situated in the hinterland of the Carpathian orogenic wedge, which occupied an upper plate position above the subducting European Plate (Fig. 1B). During the Middle Eocene, the TR was located on the forebulge side of this retroarc foreland basin (Tari et al. 1993). The flexure response of the lithosphere in such settings is commonly accommodated by hinterland-dipping normal faults developed along the outer margin of foreland basins (Scisciani et al. 2001). We interpret the Middle Eocene Környe–Zsámbék fault (Fig. 2B) as representing one of these extensional to transtensional structures (Héja et al. 2022).

The oblique dextral-reverse reactivation of the Vértessomló thrust, along with other transpressional structures overprinting the Oligocene, reflects the southward propagation of the Paleogene orogenic front within the Hungarian Paleogene retroarc basin, as suggested by Tari et al. (1993). We propose that the transition from transtension to transpression occurred around the Middle and Late Eocene boundary in the eastern part of the TR, consistent with deposition of Upper Eocene beds in a transpressional piggy-back basin of the Buda Hills (Fodor et al. 1994). The Upper Eocene succession is absent in the immediate vicinity of the quarry, where Upper Oligocene beds unconformably cover the denuded surface of Middle Eocene or Triassic rocks (infra-Oligocene denudation; sensu Telegdi-Roth 1927). The compressional or transpressional deformation continued after Oligocene sedimentation into the Early Miocene (Fodor 2008; Palotai & Csontos 2013; Fodor et al. 2018). Alternatively, Fodor et al. (2018) suggested that the Eocene transtension may have occurred locally between different sub-basins, with some areas exhibiting transpressional or compressional tectonic regimes even before the Oligocene, implying spatially and temporary variable stress fields during the Eocene.

D4 – Miocene extension

Miocene extensional structures of Strázsa Hill

The Paleogene collision of Europe and Adria was followed by the development of slab tear beneath the Eastern Alps, which subsequently propagated laterally beneath the Carpathians (Handy et al. 2015). The retreat of the subducting European slab led to subduction rollback beneath the Carpathians and induced substantial back-arc extension within the upper plate. This extensional regime led to the formation of the Miocene Pannonian Basin (Fig. 1C) (Tari et al. 1999; Horváth et al. 2015; Balázs et al. 2016, 2025; Fodor et al. 2021; Csontos et al. 2025). Structures related to the formation of the Pannonian Basin are also exposed in the quarry of Strázsa Hill.

Several normal faults cutting the basal part of the Middle Miocene deposits were observed along the northwestern and northern quarry walls (Figs. 9, 10). These faults strike between NW–SE and N–S, and were formed under ENE–WSW to E–W extension, respectively (Fig. 11D). Increased thickness of the Middle Miocene (late Badenian) deposits in the hanging wall of some normal faults, together with breccia wedges, indicate syn-sedimentary faulting (F22, F23, F25 in Fig. 10B). All these faults are sealed by younger Middle Miocene strata. The basal part of the Middle Miocene deposits also displays characteristic pre- or syn-diagenetic deformation. For example, the upward increase in offset along the F18 normal fault can be explained by differential compaction of the Middle Miocene sand across the fault (Fig. 9B). These observations suggest that all these structures were formed during the sedimentation and early diagenesis of the Middle Miocene (Badenian) sequence.

However, several normal faults also cut across the upper Middle Miocene (Sarmatian) and Upper Miocene (Pannonian) strata, such as the relatively large-offset F15 fault (Figs. 3A, 9A, B). The mixed microfossil assemblage within the fault lens of F15 was interpreted by Kercsmár et al. (2020) as evidence for infiltration of Upper Miocene sediments into the fault zone. We propose an alternative explanation, whereby the fault-bounded lens represents a mixture of unconsolidated Middle Miocene (Badenian and Sarmatian) sediments that were sheared between the footwall and hanging wall blocks of the F15 fault (Fig. 9B). In either case, the displacement of basal Upper Miocene sediments indicates that faulting continued into the Late Miocene. Onlap surfaces observed in the hanging wall of the F15 fault (Fig. 9E) may reflect the final tilting of the hanging wall rocks and thus mark the termination of normal faulting. However, the uncertain Upper Miocene to Quaternary age of the overlying succession hampers the precise determination of the fault's final activity.

We propose that the F14, F13 faults (Fig. 8B), and farther south the F9 fault (Fig. 6B), represent the southern continuation of the F15 fault, exhibiting pronounced along-strike segmentation. The map pattern (Fig. 3A) shows that fault linkages along this W- to SW-dipping fault zone coincide with inherited structures. This is particularly evident for the NE–SW-striking northern splay of the Vértessomló thrust, interpreted as a D2 structure. The sigmoidal shear fractures within tectonically smeared clay suggest normal-sense reactivation of this thrust (Fig. 8C). Furthermore, the position of the thrust between the F13 and F14 faults indicates that this segment acted as a connecting splay fault linking the Miocene normal faults. Similar relationships between Miocene normal faults and pre-existing

structures are recognizable in map-view as well (Fig. 2). Specifically, the N–S striking normal faults of the Zsámbék and Mány Basins commonly terminate against the Vértessomló thrust, where stepovers developed along this inherited structure (Héja et al. 2022). The significance of structural inheritance in Miocene normal faulting has been further emphasized by a recent study by Beke et al. (2025) in the Pilis and Buda Hills (for location see Fig. 2A). These authors propose that an oblique rift pattern formed with normal faults initially oriented slightly oblique to, and subsequently rotating perpendicular to the regional extension direction, guided by inherited E–W and NW–SE-trending Mesozoic structures.

Polyphase rifting and the role of vertical axis rotation

The structural evolution of the Pannonian Basin is traditionally divided into syn-rift and post-rift phases. According to the pioneering works of Royden et al. (1983) and Horváth & Rumpler (1984), the transition from syn-rift to post-rift conditions occurred around the Middle to Late Miocene boundary, or possibly within the Middle Miocene (Badenian) (Tari 1994; Tari et al. 1999). However, structural data of the TR (Fodor 2008; Fodor et al. 2018), including our observations at Strázsa Hill, indicate that normal faulting is not confined to the Middle Miocene but continued into the Late Miocene. Several recent studies (Balázs et al. 2016; Fodor et al. 2021, 2025) documented a progressive migration of subsidence and fault activity toward the central parts of the Pannonian Basin. Our observations are consistent with this regional trend. In the study area, subsidence and faulting began not earlier than the Middle Miocene (late Badenian), and the observed structures may represent the late stage of this migrating basin formation process (Fodor et al. 2025). In addition, some of the faults at the Strázsa Hill (e.g., F15 in Fig. 9B) appears to extend the syn-rift deformation phase into the early part of the Late Miocene.

The orientation of the observed Miocene normal faults shows considerable scatter. Based on strike direction, two main groups of faults can be distinguished: NNW–SSE and N–S (Fig. 11B–D). These fault orientations are consistent with the major map-scale normal faults of the Mány and Zsámbék Basins (Fig. 2B) (Héja et al. 2022) and with those further north in the Gerecse Hills (Fig. 2A) (Bada et al. 1996; Fodor et al. 2018). A similarly variable strike pattern of Miocene normal faults has been reported from other parts of the Pannonian Basin as well (Petrik et al. 2016; Fodor et al. 2021; Beke et al. 2025; Csontos et al. 2025). This complex fault geometry is commonly interpreted as the result of polyphase faulting caused by gradual changes of the horizontal stress axes (Csontos et al. 1991), related to counterclockwise rotation of crustal blocks and associated faults (Márton & Fodor 1995; Márton & Márton 1996).

Paleomagnetic studies by Karátson et al. (2000, 2007) provided direct evidence for variable block rotations in volcanoclastic rocks near the study area (Visegrád and Börzsöny Mts.; Fig. 2A) constrained by K–Ar ages of 15.3–15.5±0.5 Ma. More recent structural and radiometric data suggest that the main phase of rotation postdates 15.3 Ma (Beke et al. 2025). Comparable new results east of the Danube suggest that the rotation of stress axes occurred between 14.9 and 14.7 Ma (Juhász et al. 2025). In the earlier interpretation of Fodor et al. (1999), the transition from NE–SW to E–W extension was thought to have taken place between 15 and 14 Ma, whereas the NE–SW-oriented main syn-rift extension remained active during the early Middle Miocene (early Badenian) (Petrik et al. 2016; Beke et al. 2019). These studies collectively indicate a gradual shift between successive extensional regimes, most likely corresponding to the period of counterclockwise block rotations.

Based on the above considerations, we suggest that the varying orientations of the Miocene normal faults at Strázsa Hill reflect temporally distinct rifting sub-phases. Most syn-sedimentary faults within the lower part of the Middle Miocene sequence strike NNW–SSE (Fig. 11D). However, some faults show an N–S strike, although their measurement is uncertain due to their position in the upper quarry wall. These structures may represent transitional deformation (D4a sub-phase, Fig. 11D) that was contemporaneous with the rotation described above. The F15 fault, which displaces the Upper Miocene marker bed, together with parallel structures, may correspond to a younger phase of faulting (D4b sub-phase) that postdates the rotation (Figs. 11B, 13C). If these structures have regional significance, they would extend the upper time limit of the transitional period between rifting phases to the late Middle Miocene (Sarmatian), around 13 Ma. This age would be more than 1 Ma younger than previously suggested by most recent studies (Petrik et al. 2016; Beke et al. 2019; Juhász et al. 2025).

D5 – Late Miocene to Quaternary (?) strike-slip faulting

Comparison of the structural data of Strázsa Hill with neotectonic structures of the Pannonian Basin

Several N–S-striking dextral and NE–SW-striking sinistral faults, together with a few NE-dipping minor thrusts, were identified within the Upper Miocene deposits at Strázsa Hill. These fault-slip data are assigned to the D5 strike-slip tectonic phase, which represents the youngest deformation event, dated to the Late Miocene(?)–Quaternary. The N–S striking Miocene normal faults (D4) possibly underwent dextral reactivation during this phase. The D5 stress field is characterised by a NE–SE oriented σ1 axis (Fig. 11A). Similar stress fields were reported by Csontos et al. (1991), Fodor et al. (1999), and Fodor (2010), who associated them with the basin-wide deformation phase that began in the latest Middle Miocene and persisted through the Late Miocene, with local and temporal variations (see Petrik et al. 2016). Moreover, a (N)NE–(S)SW-oriented σ1 direction can be inferred from neotectonic fault patterns (Fodor et al. 2005; Ruszkiczay-Rüdiger et al. 2007; Koroknai et al. 2020; Visnovitz et al. 2021) and is consistent with recent stress trajectories (Porkoláb et al. 2023).

In addition to tectonic deformation, the F24 fault is interpreted as a gravitational slide structure (Fig. 10B). The growth strata within Quaternary deposits in its hanging wall indicate syn-sedimentary displacement (Fig. 10B).

Conclusions

A detailed structural analysis of Strázsa Hill, an exceptional key outcrop of the central Pannonian Basin, was carried out, providing new insights into the Mesozoic and Cenozoic tectonic evolution of the Transdanubian Range.

- NW–SE striking Carnian syn-sedimentary normal faults and slides represent the oldest structures (D1 phase), formed during the passive-margin evolution of the Transdanubian Range.
- Imbrication of the Triassic rock units occurred due to pre-Paleogene, probably mid-Cretaceous, south-vergent thrusting (D2 phase). The Vértessomló thrust, one of the most important Cretaceous structures of the northeastern Transdanubian Range, is exposed in the quarry. Along the main splay of the Vértessomló thrust, the Norian Fődolomit Fm. is overthrust by the Lower Carnian Inota Fm., which is in turn overthrust by the Ladinian Budaörs Dolomite Fm. along the northern splay of the thrust. The exposure of such map-view structures is unique in Hungary, considering the generally poor outcrop conditions.
- The normal-dextral reactivation of the Vértessomló thrust is likely related to Middle Eocene basin formation (D3a sub-phase). Sedimentological and structural evidence indicate a second, dextral-reverse reactivation of the thrust during and after the Oligocene, but before the onset of Middle Miocene sedimentation (D3b sub-phase). Oligocene sedimentation was controlled by this reactivation, as evidenced by an asymmetric growth syncline in the footwall. Redeposited Triassic and Oligocene sediments in the lowermost thrust sheet likely originated from the uplifted hanging wall, where the Oligocene deposits are absent and the Triassic succession is directly covered by Miocene strata.
- Several NW–SE and N–S-striking Miocene normal faults were identified (D4). Some of these structures represent Middle Miocene syn-sedimentary faults (D4a sub-phase), while others suggest that extensional deformation continued in the early Late Miocene (D4b sub-phase).
- Fault-slip data from Upper Miocene strata indicate a younger, Late Miocene to possibly recent(?) phase of strike-slip faulting (D5), characterised by NE–SW compression and NW–SE extension. Some of the N–S-striking normal faults may have been reactivated as dextral strike-slip faults during this phase.

Acknowledgements: The fieldwork is part of the geological mapping project of the Geological Survey (Supervisory Authority for Regulatory Affairs, Hungary), led by Zs. Kercsmár. This research was supported by the NKFIH grants No.139275, led by B. Beke, and No. 134873, led by L. Fodor. We would like to especially thank Hazai Bányák Zrt. for permitting us to conduct fieldwork in the quarry. We are grateful to Reviewer Dušan Plašienka and Associate Editor Rastislav Vojtko for their detailed and constructive review.

References

Albert G. 2000: Folds of the Northern Bakony, Transdanubian Range, West Hungary [Az Északi-Bakony gyűrődései]. *MSc Thesis, Eötvös Loránd University, Budapest, Department of Geology*, 1–89.

Anderson E.M. 1951: The dynamics of faulting and dyke formation with application to Britain. 2nd ed., *Oliver & Boyd*, Edinburgh, 1–206.

Angelier J. 1990: Inversion of field data in fault tectonics to obtain the regional stress – III. A new rapid direct inversion method by analytical means. *Geophysical Journal International* 103, 363–373.

Angelier J. & Manoussis S. 1980: Classification automatique et distinction des phases superposée en tectonique de failles. *Comptes Rendus de l'Académie des Sciences, Paris* 290, série D, 651–654.

Bada G., Fodor L., Székely B. & Timár G. 1996: Tertiary brittle faulting and stress field evolution in the Gerecse Mts. N. Hungary. *Tectonophysics* 255, 269–290.

Balázs A., Matenco L., Magyar I., Horváth F. & Cloetingh S. 2016: The link between tectonics and sedimentation in back-arc basins: New genetic constraints from the analysis of the Pannonian Basin. *Tectonics* 35, 1526–1559. https://doi.org/10.1002/2015TC004109

Balázs A., Oravecz É., Bartha A., Fodor L., Magyar I. & Sztanó O. 2025: Tectonostratigraphic models of an extensional back-arc basin: inferences for the evolution of the Pannonian Basin system. *Geological Society, London, Special Publications* 554. https://doi.org/10.1144/SP554-2024-8

Báldi T. 1986: Mid-Tertiary Stratigraphy and Paleogeographic Evolution of Hungary. *Akadémia Press*, Budapest, 1–293.

Báldi-Beke M. & Báldi T. 1985: The evolution of the Hungarian Palaeogene basins. *Acta Geologica Hungarica* 28, 5–28.

Balla Z. & Dudko A. 1989: Large-scale Tertiary strike-slip displacements recorded in the structure of the Transdanubian Range. *Geophysical Transactions* 35, 3–63.

Beke B., Fodor L., Millar L. & Petrik A. 2019: Depth calibration of deformation mechanism and progressive mechanism change of deformation bands /in function of burial/ (Neogene Pannonian Basin, Hungary). *Marine and Petroleum Geology* 105, 1–16. https://doi.org/10.1016/j.marpetgeo.2019.04.006

Beke B., Fialowski M., Müller T., Schubert F., Lukács R., Guillong M., Harangi Sz. & Fodor L. 2025: Extensive silicification of sandstone-hosted fault damage zones: evolution of deformation mechanism, style and fault pattern from the pre-rift to main rift phases of the Pannonian Basin. *Basin Research* 37, e70043. https://doi.org/10.1111/bre.70043

Benkő K. & Fodor L. 2002: Structural geology near Csővár, Hungary [Csővár környékének szerkezetföldtana]. *Földtani Közlöny* 132, 223–246.

Budai T. 2004: Middle Triassic basin facies and volcanites in the Zsámbék Basin, Transdanubian Range, Hungary [Középső-triász medencefáciesek és vulkanitok a Zsámbéki medencében]. *Annual Report of the Hungarian Geological Institute* 2002, 189–194.

Budai T. & Síkhegyi F. 2004: Geological Map of Hungary, 1:100.000, L–34–2 Dorog (Esztergom). *Geological Institute of Hungary*, Budapest.

Budai T. & Vörös A. 1993: Middle Triassic events of the Transdanubian Central Range in the frame of the Alpine evolution. *Acta Geologica Hungarica* 36, 3–13.

Budai T. & Vörös A. 2006: Middle Triassic platform and basin evolution of the southern Bakony Mountains (Transdanubian Range, Hungary). *Rivista Italiana di Paleontologia e Stratigrafia* 112, 359–371.

Budai T., Császár G., Csillag G. Dudko A., Koloszár L. & Majoros Gy. 1999: Geology of the Balaton Highland. Explanation to the Geological Map of the Balaton Highland, 1:50.000. *Geological Institute of Hungary*, Budapest, 1–257.

Budai T., Fodor L., Csillag G. & Piros O. 2005: Stratigraphy and structure of the southeastern part of the Vértes Mountain (Transdanubian Range, Hungary) [A Vértes délkeleti triász vonulatának rétegtani és szerkezeti felépítése]. *Annual Report of the Geological Institute of Hungary* from 2004, 189–203.

Budai T., Haas J. & Piros O. 2015: New stratigraphic data on the Triassic basement of the Zsámbék Basin — tectonic inferences [Új rétegtani adatok a Zsámbéki-medence triász aljzatából – szerkezetföldtani következtetések]. *Földtani Közlöny* 145, 247–257. https://ojs3.mtak.hu/index.php/foldtanikozlony/article/view/134

Budai T., Fodor L., Kercsmár Zs., Lantos Z., Csillag G. & Selmeczi I. 2018: Geological map of the Gerecse Mountains, 1:50.000. *Mining and Geological Survey of Hungary*, Budapest.

Cornée J.J., Moisette P., Saintmartin J.P., Dulai A., Tóth E., Görög Á., Kázmér M. & Müller P. 2009: Marine carbonate systems in the Sarmatian of the Central Paratethys: the Zsámbék Basin of Hungary. *Sedimentology* 56, 1728–1750. https://doi.org/10.1111/j.1365-3091.2009.01055.x

Császár G. 1995: An overview of the Cretaceous research in the Gerecse and the Vértes Foreland [A gerecsei és vértes-előtéri kréta kutatás eredményeinek áttekintése]. *Általános Földtani Szemle* 27, 133–152.

Császár G. & Árgyelán G. B. 1994: Stratigraphic and micromineralogic investigations on Cretaceous Formations of the Gerecse Mountains, Hungary and their palaeogeographic implications. *Cretaceous Research* 15, 417–434.

Császár G., Haas J. & Jocháné-Edelényi E. 1978: Bauxite geological map of the Transdanubian Range [A Dunántúli-középhegység bauxitföldtani térképe], 1:100.000. *Geological Institute of Hungary*, Budapest.

Császár G., Csereklei E. & Budai T. 2004: Geological Map of Hungary, 1:100.000, L–34–14 Érd (Bicske). *Geological Institute of Hungary*, Budapest.

Csicsek L.Á. & Fodor L. 2016: Imbrication of Middle Triassic rocks near Öskü (Bakony Hills, Western Hungary) [Középső-triász képződmények pikkelyeződése a bakonyi Öskü környékén]. *Földtani Közlöny* 146, 355–370.

Csillag G., Kordos L., Lantos Z. & Magyar I. 2008: Upper Miocene. In: Budai T. & Fodor L. (eds.): Geology of the Vértes Hills. Explanatory book to the Geological Map of the Vértes Hills, 1:50.000. *Geological Institute of Hungary*, Budapest, 93–106, 250–278.

Csontos L. & Vörös A. 2004: Mesozoic plate tectonic reconstruction of the Carpathian region. *Palaeogeography, Palaeoclimatology, Palaeoecology* 210, 1–56.

Csontos L., Tari G., Bergerat F. & Fodor L. 1991: Evolution of the stress fields in the Carpatho-Pannonian area during the Neogene. *Tectonophysics* 199, 73–91. https://doi.org/10.1016/0040-1951(91)90119-d

Csontos L., Dunkl I., Koroknai B., Tari G., Soós B., Magyari Á., Nyíri D., Soták J., Wórum G., Tóth T. & Kovács G. 2025: The formation and deformation of the Neogene Pannonian Basin: a structural overview. *Geological Society, London, Special Publications* 554. https://doi.org/10.1144/sp554-2023-222

Du Bernard X.D., Eichhubl P. & Aydin A. 2002: Dilation bands: A new form of localized failure in granular media. *Geophysical Research Letters* 29, 2176. https://doi.org/10.1029/2002GL015966

Dunkl I., Farics É., Józsa S., Lukács R., Haas J. & Budai T. 2019: Traces of Carnian volcanic activity in the Transdanubian Range, Hungary. *International Journal of Earth Sciences* 108, 1451–1466. https://doi.org/10.1007/s00531-019-01714-w

Erdei B., Hably L., Héja G. & Fodor L. 2022: The late Oligocene macroflora of Zsámbék, central Hungary. *Fossil Imprint* 78, 298–309. https://doi.org/10.37520/fi.2022.012

Farics É. 2018: Traces of Carnian volcanism in the Transdanubian Central Mountains and the debris of volcanic rocks in the Eocene basal beds of the Buda Hills [A karni vulkanizmus nyomai a Dunántúli-középhegységben és a vulkanitok törmeléke a Budai-hegység eocén bázisképződményében]. *PhD Thesis, Eötvös Loránd University, Budapest, Department of Geology*, 1–172.

Fodor L. 2008: Structural geology. In: Budai T. & Fodor L. (eds.): Geology of the Vértes Hills. Explanatory book to the Geological Map of the Vértes Hills 1:50.000. *Geological Institute of Hungary*, Budapest, 145–202, 282–300.

Fodor L. 2010: Mesozoic–Cenozoic stress fields and fault patterns in the northwestern part of the Pannonian Basin – methodology and structural analysis [Mezozoos–kainozoos feszültségmezők és törésrendszerek a Pannon-medence ÉNy-I részén – módszertan és szerkezeti elemzés]. *Doctoral work of the Hungarian Academy of Sciences*, 1–129, 7 appendices. https://real-d.mtak.hu/343/4/dc_63_10_doktori_mu.pdf

Fodor L. & Bíró I. 2004: Abrasional Eocene rocky shore along the Cretaceous Vértessomló Thrust (Szarvas-kút, Vértes Hills, Hungary) [Sziklás eocén tengerpart a kréta korú Vértessomlói-rátolódás mentén (Szarvas-kút, Vértes)]. *Annual Report of the Geological Institute of Hungary* from 2002, 153–162.

Fodor L., Magyari Á., Kázmér M. & Fogarasi A. 1992: Gravity-flow dominated sedimentation on the Buda paleoslope (Hungary). Record of Late Eocene continental escape of the Bakony Unit. *Geologische Rundschau* 81, 695–716.

Fodor L., Magyari Á., Fogarasi A. & Palotás K. 1994: Tertiary tectonics and Late Paleogene sedimentation in the Buda Hills, Hungary. A new interpretation of the Buda Line [Tercier szerkezetfejlődés és késő paleogén üledékképződés a Budai-hegységben. A Budai vonal új értelmezése]. *Földtani Közlöny* 124, 129–305.

Fodor L., Csontos L., Bada G., Györfi I. & Benkovics L. 1999: Tertiary tectonic evolution of the Pannonian basin system and neighbouring orogens: a new synthesis of paleostress data. In: Durand B., Jolivet L., Horváth F. & Séranne M. (eds.): The Mediterranean Basins: Tertiary extension within the Alpine Orogen. *Geological Society, London, Special Publications* 156, 295–334. https://doi.org/10.1144/GSL.SP.1999.156.01.15

Fodor L., Bada G., Csillag G., Horváth E., Ruszkiczay-Rüdiger Zs. Palotás K., Síkhegyi F., Timár G., Cloetingh S. & Horváth F. 2005: An outline of neotectonic structures and morphotectonics of the western and central Pannonian basin. *Tectonophysics* 410, 15–41. https://doi.org/10.1016/j.tecto.2005.06.008

Fodor L., Sztanó O. & Kövér Sz. 2013: Mesozoic deformation of the northern Transdanubian Range (Gerecse and Vértes Hills). *Acta Mineralogica-Petrographica, Field guide series* 31, 1–52.

Fodor L., Héja G., Kövér Sz., Csillag G. & Csicsek Á.L. 2017: Cretaceous deformation of the south-eastern Transdanubian Range Unit, and the effect of inherited Triassic–Jurassic normal faults. Pre-conference Excursion Guide, 15th Meeting of the Central European Tectonic Studies Group (CETeG) 5–8th April, 2017 Zánka, Lake Balaton. *Acta Mineralogica-Petrographica, Field guide series* 32, 47–76.

Fodor L., Kercsmár Zs. & Kövér Sz. 2018: Structure and deformation phases of the Gerecse. In: Budai T. (Ed.): Geology of the Gerecse Mountains. *Mining and Geological Survey of Hungary*, Budapest, 169–208, 370–386.

Fodor L., Balázs A., Csillag G., Dunkl I., Héja G., Jelen B., Kelemen P., Kövér Sz., Németh A., Nyíri D., Selmeczi I., Trajanova M., Vrabec M. & Vrabec M. 2021: Crustal exhumation and depocenter migration from the Alpine orogenic margin towards the Pannonian extensional back-arc basin controlled by inheritance. *Global and Planetary Change* 201, 103475. https://doi.org/10.1016/j.gloplacha.2021.103475

Fodor L., Balázs A., Oravecz É., Harangi Sz., Cloetingh S., Gerya T. & Lukács R. 2025: Migration of deformation, basin subsidence, magmatism in the extensional Pannonian Basin: good fit between numerical models and observations. In: Virág A., Cserép B., Molnár K., Szemerédi M. (eds.): 15th Assembly of Petrology and Geochemistry, Nagybörzsöny – Banská Štiavnica, 2–4 October 2025. *Book of Abstracts*, 32–35. https://geochem.hu/conf/15kgvgy/abstracts.html

Ford M., Williams E.A., Artoni A., Verges J. & Hardy S. 1997: Progressive evolution of a fault-related fold pair from growth strata geometries, Sant Llorens De Morunys, SE Pyrenees. *Journal of Structural Geology* 19, 413–441.

Főzy I. & Janssen N.M.M. 2009: Integrated Lower Cretaceous biostratigraphy of the Bersek Quarry, Gerecse Mountains, Transdanubian Range, Hungary. *Cretaceous Research* 30, 78–92.

Gawlick H.J., Lein R. & Bucur I.I. 2021: Precursor extension to final Neo-Tethys breakup: flooding events and their significance for the correlation of shallow-water and deep-marine organisms (Anisian, Eastern Alps, Austria). *International Journal of Earth Sciences* 110, 419–446. https://doi.org/10.1007/s00531-020-01959-w

Gerinczy A. 2009: Bauxite geology of the Buda Hills [A Budai-hegység bauxitföldtana]. *MSc thesis, Eötvös Loránd University, Department of Geology*, Budapest, 1–178.

Granado P., Tavani S., Carrera N. & Muñoz J.A. 2018: Deformation pattern around the Conejera fault blocks (Asturian Basin, North Iberian Margin). *Geologica Acta* 16, 357–373. https://doi.org/10.1344/GeologicaActa2018.16.4.2

Haas J. & Budai T. 2014: Stratigraphic and facies problems of the Upper Triassic in the Transdanubian Range Reconsideration of old problems on the basis of new results [A Dunántúli-középhegység felső-triász képződményeinek rétegtani- és fácieskérdései. Régi problémák újragondolása újabb ismeretek alapján]. *Földtani Közlöny* 144, 125–142.

Haas J., Oravecz J. & Góczán F. 1981: Report on the study of Zsámbék Zs–14 key-section well [Jelentés a Zsámbék, Zs–14. sz. alapszelvény fúrás vizsgálatáról]. *Manuscript, Hungarian Geological, Geophysical and Mining Database*, Budapest, inventory number 1656/29.

Haas J., Jocháné-Edelényi E., Gidai L., Kaiser M., Kretzoi M. & Oravecz J. 1984: Geology of the Sümeg Area. *Geologica Hungarica Series Geologica* 20, 353.

Haas J., Kovács S., Krystyn L. & Lein R. 1995: Significance of Late Permian–Triassic facies zones in terrane reconstructions in the Alpine–North Pannonian domain. *Tectonophysics* 242, 19–40.

Haas J., Tardi-Filácz E., Oravecz-Scheffer A. & Góczán F. 1997: Cretaceous insertions in Triassic (?) dolomites at Csővár, North Hungary. *Acta Geologica Hungarica* 40, 179–196.

Haas J., Budai T., Csontos L., Fodor L. & Konrád Gy. 2010: Pre-Cenozoic geological map of Hungary 1:500.000. *Geological and Geophysical Institute of Hungary*, Budapest.

Handy M.R., Ustaszewski K. & Kissling E. 2015: Reconstructing the Alps-Carpathians-Dinarides as a key to understanding switches in subduction polarity, slab gaps and surface motion. *International Journal of Earth Sciences* 104, 1–26.

Héja G. 2015: The tectono-sedimentological interpretation of the albian–cenomanian basin evolution of the Northern Bakony, Hungary [Az északi-bakonyi albai–cenomán üledékciklus tektono-szedimentológiai értelmezése]. *Földtani Közlöny* 145, 257–272.

Héja G., Kövér S., Csillag G., Németh A. & Fodor L. 2018: Evidences for pre-orogenic passive-margin extension in a Cretaceous fold-and-thrust belt on the basis of combined seismic and field data (western Transdanubian Range, Hungary). *International Journal of Earth Sciences* 107, 2955–2973. https://doi.org/10.1007/s00531-018-1637-3

Héja G., Kercsmár Zs., Kövér Sz., Budai T., Noui M.Y. & Fodor L. 2022: The role of rheology and fault geometry on fault reactivation: a case-study from the Zsámbék–Mány Basin, Central Hungary. *Geosciences* 2022, 12, 433. https://doi.org/10.3390/geosciences12120433

Horváth F. & Rumpler J. 1984: The Pannonian basement: extension and subsidence of an alpine orogene. *Acta Geologica Hungarica* 27, 229–235.

Horváth F., Musitz B., Balázs A., Végh A., Uhrin A., Nádor A., Koroknai B., Pap N., Tóth T. & Wórum G. 2015: Evolution of the Pannonian basin and its geothermal resources. *Geothermics* 53, 328–352. https://doi.org/10.1016/j.geothermics.2014.07.009

Juhász D., Chiara L., Benkó Zs., Sigmundsson F., Beke B., Bergerat F., Fialowski M. & Fodor L. 2025: Dyke emplacement and its interaction with fracture systems and regional stress fields: combination of a field study and geochronology in Cserhát Hills, Hungary. *Tectonophysics* 906, 230722. https://doi.org/10.1016/j.tecto.2025.230722

Kaiser M. 1997: Geomorphic evolution of the Transdanubian Mountains, Hungary. *Zeitschrift für Geomorphologie* Suppl. Bd. 110, 1–14.

Karádi V., Budai T., Haas J., Vörös A., Piros O., Dunkl I. & Tóth E. 2022: Change from shallow to deep-water environment on an isolated carbonate platform in the Middle Triassic of the Transdanubian Range (Hungary). *Palaeogeography, Palaeoclimatology, Palaeoecology* 587, 110793. https://doi.org/10.1016/j.palaeo.2021.110793

Karátson D. & Németh K. 2001: Lithofacies associations of an emerging volcaniclastic apron in a Miocene volcanic complex: an example from the Börzsöny Mountains, Hungary. *International Journal of Earth Sciences* 90, 776–794.

Karátson D., Márton E., Harangi Sz., Józsa S., Balogh K., Pécskay Z., Kovácsvölgyi S., Szakmány Gy. & Dulai A. 2000: Volcanic evolution and stratigraphy of the Miocene Börzsöny Mts., Hungary. An integrated study. *Geologica Carpathica* 51, 325–343.

Karátson D., Oláh I., Pécskay Z., Márton E., Harangi Sz., Dulai A., Zelenka T. & Kósik Sz. 2007: Miocene volcanism in the Visegrád Mountains, Hungary: an integrated approach to regional stratigraphy. *Geologica Carpathica* 58, 541–563.

Kázmér M., Dunkl I., Frisch W., Kuhlemann J. & Ozsvárt P. 2003: The Palaeogene forearc basin of the Eastern Alps and Western Carpathians: subduction erosion and basin evolution. *Journal of the Geological Society London* 160, 413–428.

Kelemen P., Dunkl I., Csillag G., Mindszenty A., Józsa S., Fodor L. & von Eynatten H. 2023: Origin, timing and paleogeographic implications of Paleogene karst bauxites in the northern Transdanubian range, Hungary. *International Journal of Earth Sciences* 112, 243–264. https://doi.org/10.1007/s00531-022-02249-3

Keller G., Li L. & MacLeod N. 1995: The Cretaceous/Tertiary boundary stratotype section at El Kef, Tunisia: how catastrophic was the mass extinction? *Palaeogeography, Palaeoclimatology, Palaeoecology* 119, 221–254.

Kercsmár Zs. 1993: Eocene scarp, Oligocene strike-slip, Tatabánya. In: Balla Z., Dudko A. & Fodor L. (eds.): Guide to pre-workshop excursion in the Transdanubian Range. *Field Guide, ALCAPA Workshop*, Hungary, 24–29.

Kercsmár Zs. 2004: The structural geological significance of the red calcites of Tatabánya [A tatabányai vöröskalcittelérek szerkezetföldtani jelentősége]. *Annual Report of the Geological Institute of Hungary* from 2002, 163–174.

Kercsmár Zs. 2005: New results on geology and basin evolution of the Tatabánya Eocene Basin, based on sedimentological and tectono-sedimentological studies [A Tatabányai Eocén Medence földtani felépítésének és fejlődéstörténetének újabb kutatási eredményei, üledékföldtani és tektono-szedimentológiai vizsgálatok alapján]. *PhD Thesis, Eötvös Loránd University, Department of Paleontology*, Budapest, 1–175.

Kercsmár Zs., Budai T., Szurominé Korecz A., Selmeczi I., Musicz B. & Lantos Z. 2020: Cenozoic formations of the Strázsa Hill at Zsámbék and its surroundings [A zsámbéki Strázsa-hegy és környékének kainozoos képződményei]. *Földtani Közlöny* 150, 129–150.

Kercsmár Zs., Fodor L. & Pálfalvi S. 2006: Tectonic control and basin evolution of the Northern Transdanubian Eocene Basins (Vértes Hills, Central Hungary). Proceedings of the 4th Meeting of the Central European Tectonic Studies Group/11 Meeting of the Czech Tectonic Studies Group/7th Carpathian Tectonic Workshop, Zakopane, Poland, April 19–22, 2006. *Geolines* 20, 64–66.

Koroknai B., Wórum G., Tóth T., Koroknai Zs., Fekete-Németh V. & Kovács G. 2020: Geological deformations in the Pannonian Basin during the neotectonic phase: New insights from the latest regional mapping in Hungary. *Earth Science Reviews* 211, 103411. https://doi.org/10.1016/j.earscirev.2020.103411

Mahboubi C.Y. & Naimi M.N. 2024: Geosites Inventory and Proposal of Georoutes throughout El Bayadh Area (Saharan Atlas, Algeria). *Geoheritage* 16, 76. https://doi.org/10.1007/s12371-024-00983-5

Maros Gy. 1988: Tectonic survey in the Vitány-vár area, W Hungary [A Vértes hegységi Vitány-vár környékének tektonikai elemzése]. *Annual Report of the Geological Institute of Hungary* from 1986, 295–310.

Márton E. & Fodor L. 1995: Combination of paleomagnetic and stress data: a case study from North Hungary. *Tectonophysics* 242, 99–114.

Márton E. & Márton P. 1996: Large scale rotation in North Hungary during the Neogene as indicated by palaeomagnetic data. In: Morris A. & Tarling D.H. (eds.): Paleomagnetism and Tectonics of the Peri-Mediterranean Region. *Geological Society, London, Special Publications* 105, 153–173.

Ortner H., Kositz A., Willingshofer E. & Sokoutis D. 2016: Geometry of growth strata in a transpressive fold belt in field and analogue model: Gosau Group at Muttekopf, Northern Calcareous Alps, Austria. *Basin Research* 28, 731–751. https://doi.org/10.1111/bre.12129

Palotai M. & Csontos L. 2013: Flexural basin reworked by salt-related pull-apart structures: the Adony Basin. *Central European Geology* 55, 147–180.

Palotai M., Csontos L. & Dövényi P. 2006: Field and geoelectric study of the Mesozoic (Upper Jurassic) occurrence at Kesztölc. *Földtani Közlöny* 136, 347–368 (in Hungarian with English abstract).

Palotai M., Pálfy J. & Sasvári Á. 2017: Structural complexity at and around the Triassic–Jurassic GSSP at Kuhjoch, Northern Calcareous Alps, Austria. *International Journal of Earth Sciences* 106, 2475–2487. https://doi.org/10.1007/s00531-017-1450-4

Palotás K. 2014: Study of Sarmatian sedimentation in the Buda Hills and its surroundings [A szarmata üledékképződés vizsgálata a Budai-hegységben és környékén]. *PhD Thesis, University of Pécs, Department of Geology and Meteorology*, 1–88.

Petrik A., Beke B., Fodor L. & Lukács R. 2016: Cenozoic structural evolution of the southwestern Bükk Mts. and the southern part of the Darnó Deformation Belt (NE Hungary). *Geologica Carpathica* 67, 83–104. https://doi.org/10.1515/geoca-2016-0005

Plašienka D. 2018: Continuity and Episodicity in the Early Alpine Tectonic Evolution of the Western Carpathians: How Large-Scale Processes Are Expressed by the Orogenic Architecture and Rock Record Data. *Tectonics* 37, 2029–2079. https://doi.org/10.1029/2017TC004779

Pocsai T. & Csontos L. 2006: Late Aptian–Early Albian syn-tectonic facies-pattern of the Tata Limestone Formation (Transdanubian Range, Hungary). *Geologica Carpathica* 57, 15–27.

Porkoláb K., Broerse T., Kenyeres A., Békési E., Tóth S., Magyar B. & Wesztergom V. 2023: Active tectonics of the Circum-Pannonian region in the light of updated GNSS network data. *Acta Geodaetica et Geophysica* 58, 149–173. https://doi.org/10.1007/s40328-023-00409-8

Prakfalvi P., Kuti L. & Síkhegyi F. 2000: Geological Map of Hungary, 1:100.000, L–34–3 Vác. *Geological Institute of Hungary*, Budapest.

Royden L.H., Horváth F., Nagymarosy A. & Stegena F. 1983: Evolution of the Pannonian Basin System. 2. Subsidence and thermal history. *Tectonics* 2, 91–137.

Ruszkiczay-Rüdiger Zs., Fodor L. & Horváth E. 2007: Neotectonics and Quaternary landscape evolution of the Gödöllő Hills, Central Pannonian Basin, Hungary. *Global and Planetary Change* 58, 181–196. https://doi.org/10.1016/j.gloplacha.2007.02.010

Sasvári Á. 2008: Shortening-related deformations in the Gerecse Mts., Transdanubian Range, Hungary [Rövidüléshez köthető deformációs jelenségek a Gerecse területén]. *Földtani Közlöny* 138, 385–402.

Sasvári Á. 2009: Middle Cretaceous contractional deformation and structural burial in the Gerecse Mts. *PhD thesis. Eötvös Loránd University, Department of Geology*, Budapest, 1–146.

Scharek P., Császár G. & Csereklei E. 2000: Geological Map of Hungary, 1:100.000, L–34–15. *Geological Institute of Hungary*, Budapest.

Schmid S.M., Bernoulli D., Fügenschuh B., Matenco L., Schefer S., Schuster R., Tischler M. & Ustaszewski K. 2008: The Alpine–Carpathian–Dinaridic orogenic system: Correlation and evolution of tectonic units. *Swiss Journal of Geosciences* 101, 139–183. https://doi.org/10.1007/s00015-008-1247-3

Scisciani V., Calamita F., Tavarnelli E., Rusciadelli G., Orig G.G. & Paltrinieri W. 2001: Foreland-dipping normal faults in the inner edges of syn-orogenic basins: a case from the Central Apennines, Italy. *Tectonophysics* 330, 211–224.

Sotiriou P. & Nunes P. 2024: The Geoheritage of Madeira: Implications for Natural Heritage and Geotourism. *Geoheritage* 16. https://doi.org/10.1007/s12371-024-00982-6

Stüwe K. & Schuster R. 2010: Initiation of subduction in the Alps: Continent or ocean? *Geology* 38, 175–178. https://doi.org/10.1130/G30528.1

Szabó I. & Ravasz Cs. 1970: Investigation of the Middle Triassic Volcanics of the Transdanubian Central Mountains, Hungary. *Annales Historico-Naturales Musei Nationalis Hungarici*, *Pars Mineralogica et Palaeontologica* 62, 31–52.

Szives O., Fodor L., Fogarasi A. & Kövér Sz. 2018: Integrated calcareous nannofossil and ammonite data from the upper Barremian–lower Albian of the northeastern Transdanubian Range (central Hungary): stratigraphical implications and consequences for dating tectonic events. *Cretaceous Research* 91, 229–250. https://doi.org/10.1016/j.cretres.2018.06.005

Sztanó O., Magyar I., Szuromi-Korecz A. & Sebe K. 2024: Endrőd Marl Formation. In: Babinszki E., Piros O., Csillag G., Fodor L., Gyalog L., Kercsmár Zs., Less Gy., Lukács R., Sebe K., Selmeczi I., Szepesi J., Sztanó O. & Tóth E. (eds.): Lithostratigraphic units of Hungary II. Cenozoic formations. *Supervisory Authority for Regulatory Affairs and the Stratigraphic Subcommittee of the Geological Scientific Committee of the Hungarian Academy of Sciences*, 124–125. https://sztfh.hu/downloads/foldtan/cenozoic_online.pdf

Tari G. 1994: Alpine Tectonics of the Pannonian Basin. *PhD Dissertation, Rice University*, Houston, 1–501.

Tari G. & Horváth F. 2010: Eo-Alpine evolution of the Transdanubian Range in the nappe system of the Eastern Alps: revival of a 15 years old tectonic model [A Dunántúli-középhegység helyzete és eoalpi fejlődéstörténete a Keleti-Alpok takarós rendszerében: egy másfél évtizedes tektonikai modell időszerűsége]. *Földtani Közlöny* 140, 483–510.

Tari G., Báldi T. & Báldi-Beke M. 1993: Paleogene retroarc flexural basin beneath the Neogene Pannonian Basin: a geodynamical model. *Tectonophysics* 226, 433–455.

Tari G., Dövényi P., Dunkl I., Horváth F., Lenkey L., Stefanescu M., Szafián P. & Tóth T. 1999: Lithospheric structure of the Pannonian basin derived from seismic, gravity and geothermal data. In: Durand B., Jolivet L., Horváth F. & Séranne M. (eds.): The Mediterranean Basins: Tertiary extension within the Alpine Orogen. *Geological Society Special Publications* 156, 215–250.

Telegdi-Roth K. 1927: Spuren einer Infraoligozänen Denudation am nordwestlichen Rande des Transdanubischen Mittelgebirges. *Földtani Közlöny* 57, 117–128.

Véghné Neubrandt E., Fáyné Tátray M., Mensáros P. & Balásházy L. 1978: Geological problems concerning the basin deposits and bedrocks underlying the Nagyegyháza – Mány Coal Measures in Hungary [A Nagyegyháza-mányi terület kőszénfekvő képződményeinek és alaphegységének földtani kérdései]. *Földtani Közlöny* 108, 7–17.

Visnovitz F., Jakab B., Czecze B., Hámori Z., Székely B., Fodor L. & Horváth F. 2021: High resolution architecture of neotectonic fault zones and post 8 Ma deformations in western Hungary: Observations and Neotectonic Characteristics of the Fault Zone at the Eastern Lake Balaton. *Global and Planetary Change* 203, 103540. https://doi.org/10.1016/j.gloplacha.2021.103540

Wein Gy. 1977: Tectonics of the Buda Hills [A Budai-hegység tektonikája]. *Occasional Publications of the Geological Institute of Hungary*, 1–76.